NEUTRON INTERACTION TOOL, PyNIC, FOR ADVANCED APPLICATIONS IN NUCLEAR POWER, NUCLEAR MEDICINE, AND NUCLEAR SECURITY

by

Gregory Bruce Moffitt

A thesis submitted to the faculty of
The University of Utah
in partial fulfillment of the requirements for the degree of

Master of Science

in

Nuclear Engineering

Department of Civil and Environmental Engineering

The University of Utah

December 2014

The University of Utah Graduate School

STATEMENT OF THESIS APPROVAL

The thesis of **Gregory Bruce Moffitt**

has been approved by the following supervisory committee members:

Tatjana Jevremovic	, Chair	**9/2/2014** Date Approved
Robert D. Stewart	, Member	**9/2/2014** Date Approved
Scott Miller	, Member	**9/2/2014** Date Approved

and by **Michael Barber** , Chair/Dean of

the Department/College/School of **Civil and Environmental Engineering**

and by David B. Kieda, Dean of The Graduate School.

ABSTRACT

A neutron interaction simulation tool, PyNIC, was developed for the calculation of neutron activation products and prompt gamma ray emission from neutron capture, neutron inelastic scattering, and fission interactions. This tool was developed in Python with a graphical user interface to facilitate its easy applications. The tool was validated for neutron activation analysis of a number of samples irradiated in the University of Utah TRIGA Reactor. These samples included nickel wire and the NIST standard for coal fly ash. The experimentally determined isotopes for coal fly ash were ^{56}Mn, ^{40}K, and ^{139}Ba. The samples were irradiated at reactor power levels from 1 kW to 90 kW, and the average percent difference between PyNIC estimated and laboratory measured values was 4%, 24%, 38%, and 22% for ^{64}Ni, ^{56}Mn, ^{40}K, and ^{139}Ba, respectively. These differences are mainly attributed to calibration of the high-purity germanium detector and too short of count times. The PyNIC tool is applicable to neutron activation analysis but also can find its applications in nuclear power, nuclear medicine, and in homeland security such as predicting the contents of explosives and special nuclear materials in samples of complex and unknown origins.

This work is dedicated to my wife for her love and patience through these many years of school.

TABLE OF CONTENTS

LIST OF TABLES

ACKNOWLEDGEMENTS

I would like to thank the many people who have contributed to this work and made it possible. Especially, I would like to thank my Advisor, Prof. Tatjana Jevremovic, for her guidance and inspiration throughout this entire project. Her energy and excitement for the project has been a great motivator towards its completion. I am grateful to government agencies, the U.S. Nuclear Regulatory Commission and the Department of Energy Nuclear Engineering University Programs, for being the recipient of their highly prestigious fellowships. And finally, I thank Prof. Robert Stewart and Prof. Scott Miller for serving as members of my Master's Committee.

CHAPTER 1

INTRODUCTION

1.1 Motivation

After the discovery of the neutron by James Chadwick in 1932, one of the earliest applications of neutrons was to create interactions that will possibly complete Mendeleev's periodic table (*1*). The production of radioactive isotopes through neutron capture allowed Enrico Fermi and Emilio Segre to identify elements needed to complete the periodic table, for which Fermi was awarded the Nobel Prize in 1938. Since then, neutron interactions represent the base principles of many devices used in a wide range of applications ranging from petroleum exploration to cement production to power generation and exploration of space. Neutron sources have great potential in helping to solve many of the growing needs of the world in energy development, security, and medicine. Nuclear reactors help provide a carbon neutral form of electricity generation, while neutron generators can help nuclear power to flourish through uses in nuclear waste assaying. Neutron sources, such as compact neutron generators or ^{252}Cf sources could also be used as a means to detect explosives and nuclear weapons—two applications of interest to homeland security. Neutron sources, especially compact neutron sources could provide an important role in neutron capture therapy for cancer by providing a low cost, hospital-friendly neutron source. In order for the continued growth

of the use of neutrons in these various industries, accurate modeling of neutron interactions caused by these sources combined with a thorough analysis of their applications will lead to new or improved uses in these important fields.

1.2 Thesis Objectives

The objective of this thesis was to develop a comprehensive tool to determine the gamma signatures emitted from neutron radiative capture and inelastic scattering applicable to various disciplines. The accuracy of this simulation tool is determined through comparisons of calculated activities and dose rates to neutron activation analysis (NAA) experiments performed in the University of Utah TRIGA reactor. The potential applications of the simulation tool to a range of fields such as fast neutron interrogation of used fuel, neutron capture therapy of cancer, explosives detection, and special nuclear material detection is discussed.

1.3 Organization of the Thesis

A description of neutron interactions and applications to the importance of compact neutron sources in nuclear waste assaying, neutron capture therapy, and nuclear security is given in Chapter 2. Chapter 3 is a thorough description of the PyNIC simulation tool for simulating the gamma emissions from neutron interactions in a given sample. Description of an analysis of the accuracy of the PyNIC simulation tool is verified through comparisons to NAA experiments in Chapter 4. The modeling approach necessary for each of these applications is described in Chapter 5. Chapter 6 summarizes

the main conclusions from the study and discusses the future direction of PyNIC development and application.

CHAPTER 2

NEUTRON INTERACTIONS FUNDAMENTALS AND APPLICATIONS

2.1 Fundamentals of Neutron Interactions

Neutron interactions important to nuclear power, nuclear medicine, and applications in homeland security include neutron capture; neutron scattering, both elastic and inelastic; and fission. A description of these interactions is given in this section as the fundamentals to the development of PyNIC and its potential applications.

Neutron capture involves the absorption of a neutron by a nucleus and the formation of a new nucleus. An example would be the absorption of a neutron by ^{65}Cu to form ^{66}Cu. In this case, ^{66}Cu would be referred to as the activation product. Neutron capture is also frequently referred to as radiative capture because gamma rays are produced in the majority of these absorptions (*15*). In many cases, the activation production is radioactive and will undergo additional forms of decay. This decay can be accompanied by the emission of gamma rays, which will be specific to that activation product and can be used to identify it. Typically, radiative capture cross sections, which are essentially the probability that radiative capture will occur for an interaction with a neutron of a given energy, are greater for low energy neutrons. Inelastic scattering involves the formation of a compound nucleus between the incident neutron and the target, followed by the release of a neutron at lower energy as shown in Fig. 2.1. The compound nucleus

is in an excited state from the energy of the incident neutron. Therefore for inelastic scattering to occur, the incoming neutron has to have enough energy to place the nucleus in one of these excited states. This minimum energy needed is called the threshold energy, which is different for every nuclide. For elements with moderate or high mass numbers this threshold value is generally somewhere between 0.1 to 1 MeV (*15*). The threshold energies for lower mass elements are generally much higher than for moderate or heavy elements. After the emission of a lower energy neutron, the nucleus is still in an excited state. To arrive at its ground state again, the nucleus releases a gamma ray with an energy corresponding to the excitation energy of the nucleus. Fission occurs when the nucleus splits into two smaller nuclei. Fission is typically neutron-induced and occurs in heavy isotopes such as ^{235}U and ^{239}Pu. Spontaneous fission does occur in some isotopes such as ^{240}Pu and ^{252}Cf (*15*). The fission process yields a lot of energy, mainly manifested in the kinetic energy of the fission fragment nuclei. It also yields two to three neutrons and a number of gamma emissions. The fission products are radioactive and are produced with known distributions based on the original isotope they came from. The gamma decays from these fission products provide a means for their detection through gamma-ray spectroscopy, which allows for the original fissile material to be determined by comparing with known distributions.

The gamma emissions from inelastic scattering and radiative capture are unique to a given nuclide and can be used to measure the content of this nuclide in the sample. Therefore, after irradiating the sample with a pulse of neutrons, gamma emissions are measured using a gamma detector that can distinguish between different gamma energies. A high purity germanium spectrometer is a common choice because of the high energy

resolution that can be achieved, thereby allowing for better identification of specific nuclides.

2.2 Neutron Source Fundamentals

Neutron generation occurs through many different devices ranging from ^{252}Cf neutron sources to large nuclear power generating reactors. While an exhaustive description of all the neutron source devices available in the nuclear industry would be beyond the scope of this thesis, a detailed description of compact neutron generators is included to demonstrate the applicability and usefulness of PyNIC.

A compact neutron source generates neutrons using low-energy nuclear reactions and contains three fundamental component used to generate neutrons: an ion source, an accelerator, and a target. These components are highly variable and are based on the type of reaction being used. The two most common reaction types used in compact neutron generators are the deuteron-deuterium (D-D) reaction and the deuteron-tritium (D-T) reaction.

The D-D reaction uses a source of deuterons (^{2}H ions) and a target loaded with deuterium (^{2}H atoms). The deuterons are typically accelerated to an energy in the range of a few hundred keV (*2*). These ions are accelerated towards the target, which is usually a metal hydride (*3*). A common target material is a titanium hydride target loaded with deuterium atoms. The D-D reaction cross section does not have a peak value in the low energy range but does steadily increase from 100 keV to 500 keV with all values in that range being below 100 mb. This neutron generating reaction is

$$^{2}H + {}^{2}H \rightarrow {}^{3}He + n \quad (2.1)$$

The neutrons generated through this low-energy nuclear reaction have energy of approximately 2.5 MeV (*3*).

The D-T reaction uses a source of deuterons and a target loaded with tritium (^{3}H). In a D-T generator, typically only deuterons are accelerated because it limits the tritium to the target and prevents the contamination that would otherwise occur throughout the entire generator. The cross section for the D-T reaction has a maximum value of 5 barns for a deuteron energy of 107 keV (*2*). The D-T reaction that occurs is

$$^{2}H + {}^{3}H \rightarrow {}^{4}He + n \quad (2.2)$$

The neutrons generated through this low-energy nuclear reaction have energy of approximately 14.1 MeV (*3*). The D-T reaction also has a neutron yield that is on the order of 100 times greater than the D-D reaction (*4*). The advantage to using the D-D reaction would be avoiding contamination risk from the use of tritium, which can cause serious internal damage if ingested.

Neutron yields can vary greatly depending on the ion source and reaction type. The most common ion source used in compact neutron generators is the cold-cathode, or Penning ion source (*3*). This source contains two cathode plates placed at each end of a hollow cylindrical anode. An external magnet generates a coaxial field of a few hundred gauss. The deuterium gas is at low pressure in the anode, and the electric field ionizes the deuterium. The deuterium ions then enter the accelerator portion of neutron generator

through a hole in one of the cathode plates. The Penning source is the most common source because of its simple design and durability (*3*). Radiofrequency (RF) plasma sources are another ion source commonly used in compact neutron generators. One major advantage to an RF plasma source is that it can produce much higher neutron output compared to other portable neutron generators (*5*). The RF-induction method (used in RF plasma sources) creates a higher percentage of atomic ion species compared to the Penning source, which leads to higher efficiencies because a purely atomic ion beam increases neutron production the target by 3 to 4 times that of a purely molecular ion beam (*5*). Also, while the popularity of the Penning source has been attributed to its durability (*3*), the RF source has been stated to have a longer life than the Penning source (*5*). Compact neutron sources that use a RF plasma source can generate neutrons at a rate greater than 10^{10} n/s using the D-D reaction (*5*), and these production rates would be increased using the D-T reaction.

2.3. Neutron Activation

The PyNIC algorithm is developed to provide the neutron activation estimates using the following equation for a user-specified sample composition and neutron beam parameters:

$$A_D(t) = A_{\%}(1-e^{-\lambda_D t_{irr}})e^{-\lambda_D t_{decay}} m \frac{N_A}{A_m} \int_0^\infty dE\Phi(E)\sigma_p(E) \tag{3.1}$$

$\Phi(E)$ – *fluence of neutrons with kinetic energy E (n/(cm^2*s)*

$\sigma_p(E)$ – *parent nuclide radiative capture cross section for neutrons with kinetic energy E*

(cm^2)

m – mass of sample (g)

N_A – Avogadro's number

A_m – atomic mass (g/mole)

$A_{\%}$ - atomic abundance ratio

t_{irr} – irradiation time (s)

t_{decay} – decay time (s)

$A_D(t)$ – activity of daughter isotope (Bq)

λ_D – decay constant of daughter isotope (s^{-1})

If a user were to enter a 0.05 g sample that is 100% ^{65}Cu (which activates to ^{66}Cu with a half-life of 5.12 minutes), with an irradiation time of 1 minute and a decay time of 5 minutes, and selected the thermal irradiator (TI) port of the TRIGA reactor at 10 kW as the neutron beam (see Fig. 2.2 for the neutron fluence and ^{65}Cu cross section vs. energy used in the calculations), the PyNIC would calculate the activation as follows:

$$A_D(t) = \frac{(1)0.05\ g\left(\frac{\frac{6.023x10^{23}atoms}{mol}}{65\frac{g}{mol}}\right)\left(1-e^{-\frac{ln2}{5.120min}1\ min}\right)e^{-\frac{ln2}{5.120min}5min}}{\frac{3.7x10^{7}Bq}{mCi}} \int_0^{10\ MeV} dE\Phi(E)\sigma_p(E) = 0.086\ mCi \quad (3.2)$$

The activation equation is only calculated for the selected parent isotope (^{65}Cu in this example) to the first daughter product (^{66}Cu in this example) and makes the assumption

that the daughter product is not going to absorb a neutron and activate to a second daughter (which would be ^{67}Cu in this example) before it decays.

2.3.1 Nuclear Waste Assaying

Nuclear waste assaying is an important part of short and long term storage of used nuclear fuel. Critical information such as external dose rates, special nuclear material (SNM)[1] content, and the content of a number of different radionuclides must be known so that the material can be safely transported, stored, and eventually disposed of in a long-term nuclear waste site (*6*). Methods for nuclear waste assaying include passive gamma assay, passive neutron assay, and active neutron interrogation (*6*). Passive gamma assay, which uses a gamma spectrometer to measure any gammas being emitted from a sample, is important for determining the external dose rates for the used fuel, while passive neutron measurement is used for determining the plutonium, curie, and californium content in the fuel. Knowing the dose rates obtained through passive gamma counting is important so that adequate shielding is used in transportation and storage. The shortcoming of passive techniques is that the intense gamma-ray emissions from long-lived fission products and the neutron emission from actinides prevents them from being useful in obtaining the fissile material content. Therefore, active neutron interrogation is used to determine the fissile material (^{235}U and ^{239}Pu) content in used fuel. The fissile content is important so that criticality safety is maintained through transport, storage, or processing. The fissile material content is also important in fuel reprocessing to account for material, thereby preventing plutonium from being diverted and stolen for use in

[1] SNM is nuclear material such as Uranium or Plutonium that can potentially be used to make nuclear weapons.

nuclear weapons.

Active neutron interrogation (ANI) is accomplished by irradiating the sample, in this case used nuclear fuel, with an external source of neutrons. These neutrons are used to induce fission in the fissile material, which then emits secondary neutrons that are measured by a detector. ANI is needed (instead of passive neutron assay) to measure the plutonium content within any samples that also contain californium or curium. ANI is also needed if the ^{235}U content needs to be measured. Also, when using ANI it is highly important that the energy spectrum of the incoming neutron beam is ideal for the fuel rod being interrogated. The isotopes ^{235}U and ^{239}Pu have high fission cross sections for thermal neutrons (~0.025 eV). Therefore, ideally the neutrons in the beam should be low energy by the time they reach the fuel to induce fission at the highest rate possible (while maintaining criticality safety). On the other hand, if the neutrons are already at thermal energy as they pass through any surrounding material, there is a high probability that they will be absorbed through radiative capture before reaching the fuel by materials such as iron or hydrogen. A comparison of the fission cross sections for ^{235}U and ^{239}Pu to the capture cross sections for iron and hydrogen are shown in Fig. 2.3. The cross sections for radiative capture in ^{56}Fe and ^{1}H, while not as high as the cross sections for fission in ^{235}U and ^{239}Pu, are large enough that they need to be considered because of the low-energy neutrons that will be lost through absorption. Beam design can also be further complicated when fuel is encapsulated in cement shielding because of the high hydrogen content (*6*). Avoiding parasitic absorption in the shielding and any other materials surrounding the fuel is important in ANI to allow the highest amount of neutrons to reach the fuel. When these neutrons do reach the fuel and induce fission, fast neutrons (~2

MeV) are generated. These fast neutrons have a high probability of escaping from the fuel and surrounding material and arriving at a detector.

There are a few different active neutron interrogation detector systems. One common type, a differential die-away system, uses a 14 MeV, pulsed neutron beam to irradiate the sample (*6*). These 14 MeV neutrons are moderated down to thermal energies quickly (~10 μs), and the resulting thermal neutrons have a lifetime in the range of hundreds of microseconds (*6*). The detector in this system is sensitive to fast neutrons, which are emitted during fission, but not to thermal neutrons. Also, neutrons are only counted after an interval of time in which all the neutrons from the initial pulse are thermal and all fast neutrons counted are from fission (*7*). Therefore the detector output will be proportional to the amount of fissile material and will not be contaminated by scattered thermal neutrons or initial source neutrons. For a 15 minute measurement using a pulsed neutron tube with an output of 10^8 n/s, this type of detector has a limit of detection of a few mg of Pu or ^{235}U for a 200 L waste drum containing waste with a bulk density between 0 to 1 g/cm^3 (*6*).

A second detector type is a Californium Shuffler (*6*). This detector irradiates the waste drum for a few seconds with a californium spontaneous fission source and then removes this source and counts the delayed neutrons. This is repeated a number of times until the statistics give a sufficient accuracy. For a 10 minute measurement using a ^{252}Cf source emitting 10^9 n/s, this detector system has a limit of detection of a few tens of milligrams of Pu or ^{235}U for a 200 L waste drum containing waste with a bulk density between 0 to 1 g/cm^3 (*6*). The detection limits for both types of active neutron interrogation are much better than what is achievable with passive gamma counting,

which has a detection limit of a few grams of plutonium (*6*).

In a recent study (*8*), the use of high-energy delayed gamma ray emissions (HEDGS) has also been investigated as a method for directly measuring the ^{235}U, ^{239}Pu, and ^{241}Pu content in spent fuel assemblies. While all of the forms of active waste assay are important, the use of HEDGS is the most relevant to application of the tool developed in this work. To obtain the relative concentrations of ^{235}U, ^{239}Pu, and ^{241}Pu using HEDGS from fission products involves a number of steps. The first step is irradiating spent fuel with a pulse neutron source (such as a compact neutron generator) to induce fission in ^{235}U, ^{239}Pu, and ^{241}Pu, which each have a unique distribution of fission product nuclei (*8*). The short lived gamma emitting fission products are then measured using gamma spectroscopy. The distribution of these fission products is then fit to known fission-product yield curves for ^{235}U, ^{239}Pu, and ^{241}Pu to determine the original content of each one. A plot of the distribution of fission products for thermal fission of ^{235}U, ^{239}Pu, and ^{241}Pu is shown in Fig. 2.4.

As shown in Fig. 2.4, the fission product yield for isotopes with mass numbers between 90 and 110 can be used to differentiate between uranium and plutonium fission (*8*). The region between 130 to 140 can be used to calculate the total amount of fissile material in the fuel element (*8*). A few of the key isotopes to measure using gamma spectroscopy within the 90 to 110 range are ^{90}Rb, ^{90m}Rb, and ^{95}Y (*8*).

A number of modeling steps were performed in this work (*8*) to model the fission product content for different fuel burn up levels. Also, the gamma spectra was generated from these fission products at different burn up levels. Ratios between key isotopes produced in these simulations were used to calculate the ratios of ^{235}U, ^{239}Pu, and ^{241}Pu.

Results show accuracies less than 7% can be achieved for ^{235}U, ^{239}Pu, and ^{241}Pu assuming the use of a single collimated high purity germanium detector, D-T generator of approximately 4e10 n/s, and a total assay time of 100 minutes (*8*). In summary, the use of HEDGS for fissile material content measurement is promising but would benefit from additional research.

2.3.2 Neutron Capture Therapy

Neutron capture therapy (NCT) for cancer treatment was first proposed in the years following the discovery of the neutron by James Chadwick in 1932. One of the most common forms of NCT is boron neutron capture therapy (BNCT) because of the high absorption cross section of boron-10 for thermal neutrons: 3,846 barns at 0.025 eV and 300 K (*9*). BNCT is a binary targeted therapy performed in a multistep treatment. First, a patient is given a boron-10-laced pharmaceutical selectively targeted at tumor cells. Once enough time has passed for most of the boron-10 to travel to the tumor (can vary significantly depending on how it is administered) and the highest tumor-to-healthy-tissue ratio of boron has been achieved, the tumor is irradiated with an epithermal neutron beam. These neutrons are then moderated to thermal energies as they travel through the first few cm of tissue before reaching the tumor. Thermal neutrons are then absorbed by the boron-10 and induce the nuclear reaction

$$^{10}B + n \rightarrow {}^{7}Li + \alpha + \gamma \qquad (2.3)$$

The alpha particle and Li ion have very high linear energy transfer[2] and only travel approximately the width of a cell. The DNA damage from the alpha particle and Li ion

[2] "Linear energy transfer: The rate of energy loss along the track of ionizing particle, usually expressed keV/μm" (*39*).

can induce cancer cell death. This makes BNCT a promising treatment option for cancer (under ideal conditions) because the short ranges of the alpha particle and Li ion cause most of the dose and cell damage to be localized in the tumor, thereby significantly reducing the dose to surrounding healthy tissue compared to traditional X-ray treatment. Apart from sparing healthy tissue, advantages to BNCT also include significantly shorter treatment times (as short as one treatment because of the high amount of dose delivered selectively to the tumor) and its ability to treat recurrent cancers that are normally more resistant to X-rays. With conventional X-ray radiation therapy, patients with recurrent breast cancer have fewer treatment options because nearby health tissues may have already received the accepted tolerance dose. In such situations, a second course of radiation therapy with X-rays may have unacceptably high normal tissue toxicity. BNCT may provide another option for individuals in this situation in the future if proven effective.

The source of neutrons for NCT has historically been nuclear fission reactors (*10*). This is mainly due to their ability to generate thermal or epithermal neutron beams with sufficient flux to be effective in NCT. However an existing hospital, or even a new hospital, would have a difficult time building and operating a nuclear reactor due to the cost, regulation, large size, and safety considerations involved. If proven effective, a compact neutron source on the other hand would provide the needed source in a much cheaper and easier to maintain form. The use of compact neutron generators for NCT is not unique to this work, although these researchers are the first to investigate the use of compact neutron generators for BNCT of breast cancer testing positive for human epidermal growth factor receptor 2 (HER2).

Research into the use of BNCT for HER2 positive breast cancer began in 2006 (*11*). Statistics show that 1 in every 8 women will be diagnosed with breast cancer in her lifetime (*12*). About 20% of all breast cancers are HER2 positive (*13*). The HER2 gene helps in cell growth and division and helps in cell self-repair (*12*). This makes breast cancers that are HER2 positive more aggressive and have a higher risk of recurrence (*12*). BNCT therefore is a very promising treatment for HER2 positive because it offers the possibly of shorter irradiation, better outcomes, and gives the option for additional treatments for recurrent cancers.

2.3.3 Nuclear Security

The terrorist events of September 11, 2001, demonstrated the great importance of homeland security measures needed at airports, shipping ports, and high risk establishments. Major components of these homeland security measures are explosives detection and SNM detection in airports and shipping ports. The accurate and rapid detection of these materials are crucial to the safety of the aviation industry and to the safety of the American public. In particular, the detection of highly-enriched uranium or plutonium is an extremely high priority because a nuclear weapon detonation in a large city would lead to thousands of deaths and major economic repercussions. Therefore, further development of existing and new methods for detecting these materials will help lead to a safer country and world.

2.3.3.1 Explosives Detection

The material compositions of different explosives vary significantly. Most military and commercial explosives have high nitrogen content, which can be used as a key indicator for the presence of these explosives. Homemade explosives on the other hand, which are commonly made by terrorists, do not necessarily have high nitrogen content. This makes the detection of explosives very difficult because one method will not necessarily work across every form of explosive. Therefore, the development of multiple methods is necessary and very valuable to achieve the best detection possible.

The detection of explosives is currently done primarily by using both X-ray methods and trace explosive residue methods (*14*). X-ray methods give the density and the shape of any objects being scanned, and for dual-energy X-rays an idea of the average atomic number of the material can be ascertained. Neutron-based detection methods, while not commonly used in the aviation industry, also hold great potential. Explosives detection using neutrons has an advantage over X-ray methods as it gives the elemental composition of the material (*14*).

Neutron interrogation of materials such as explosives is based on the nuclear interactions that occur between the neutrons and nuclei of the material. The nuclear interactions include inelastic scattering, radiative capture, and with some nuclides fission. The probabilities for each type of interaction are based on nuclear cross sections, which are unique for each different atomic nuclei and incoming neutron energy. Similar to nuclear waste assaying, potential neutron sources for materials detection include ^{252}Cf sources and D-D and D-T neutron generators. A ^{252}Cf source generates neutrons through spontaneous fission and can achieve high neutron generation rates around 10^9 n/s. The

disadvantage to ^{252}Cf sources is that they cannot operate in pulse mode. D-D and D-T generators are therefore more useful in most cases because they can be operated in pulse mode. Also of importance is the energy spectrum of the neutrons being generated by each source. The ^{252}Cf source produces a spectrum of neutrons with an average energy of about 2 MeV (*16*), while the D-D and D-T neutron generators yield monoenergtic neutrons of approximately 2.5 MeV and 14.1 MeV, respectively. The neutrons from these different sources are therefore going to undergo different interactions with the materials being scanned using active interrogation. To detect carbon and oxygen, the incoming neutrons would need to undergo inelastic scattering with their nuclei, and the threshold for these interactions are for an incoming neutron energy of 4.8 MeV and 6.5 MeV, respectively (*16*). Therefore, only neutrons from the D-T neutron generator can undergo these interactions.

While the cross sections for inelastic scattering only exist for high energy neutrons, cross sections for radiative capture by isotopes like nitrogen, hydrogen, and chlorine are much higher for low energy neutrons. This makes the lower energy neutrons from ^{252}Cf and the D-D neutron generator more ideal for these interactions because they start at a lower energy and are more likely to be moderated to thermal energies. A combination of a D-T source with a depleted uranium reflector is used in a model proposed by Koltick and McConchie to create a spectrum ideal for both types of interactions (*16*). In this model, neutrons emitted in the opposite direction from the target induce fission in the depleted uranium, thereby creating neutrons with an energy spectrum similar to the ^{252}Cf source. This, therefore, produces a neutron spectrum more ideal for both inelastic scattering (from the 14.1 MeV neutrons emitted from the D-T source) and radiative

capture (neutrons emitted from ^{238}U fission).

2.3.3.2 Special Nuclear Materials Detection

Detection of SNM is based on a number of methods, which include passive gamma assay, passive neutron assay, and active neutron interrogation. The gamma emissions measured in passive gamma assay of highly-enriched uranium are the 0.186 MeV gamma ray from ^{235}U and the 0.766 MeV and 1.001 MeV gamma rays from ^{234m}Pa decay (*17*). Passive gamma assay can be an effective method for detecting highly enriched uranium when the material is only lightly shielded (0.5 cm of lead) (*17*). The use of active neutron interrogation on the other hand has the ability to detect highly enriched uranium even with the use of heavier shielding.

To use active neutron interrogation for special nuclear material, a pulsed neutron source such as a D-D or D-T generator would be used to irradiate the container (*17*). This container could be anything from a shipping container to a vehicle suspected of containing special nuclear material. The goal is to induce fission in the special nuclear material, which will increase the emission of neutrons and gamma rays from the materials. This will increase the detectable signature being emitted from the sample through fission and from fission product decays, thereby overcoming detection problems due to shielding around the sample.

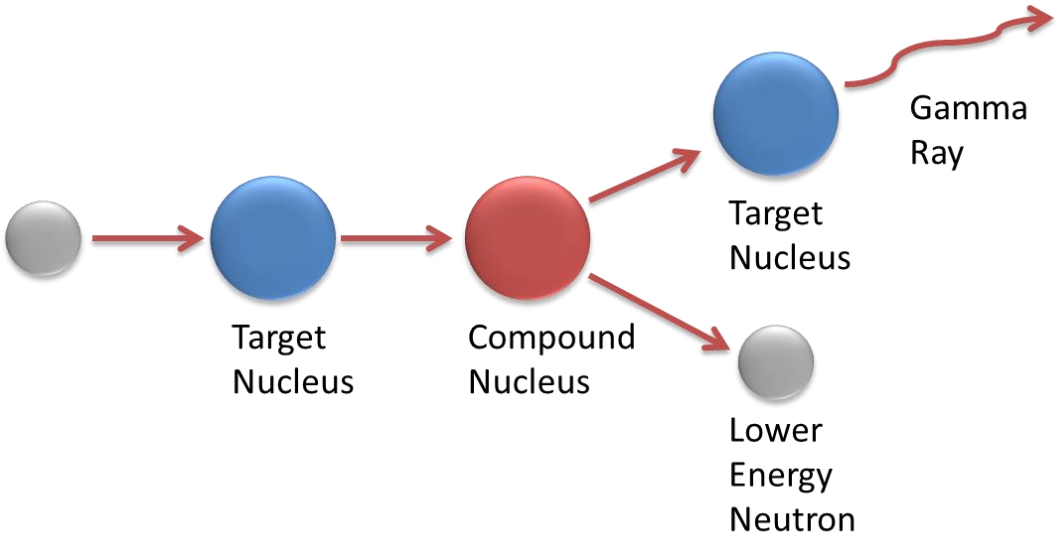

Figure 2.1. Neutron inelastic scattering

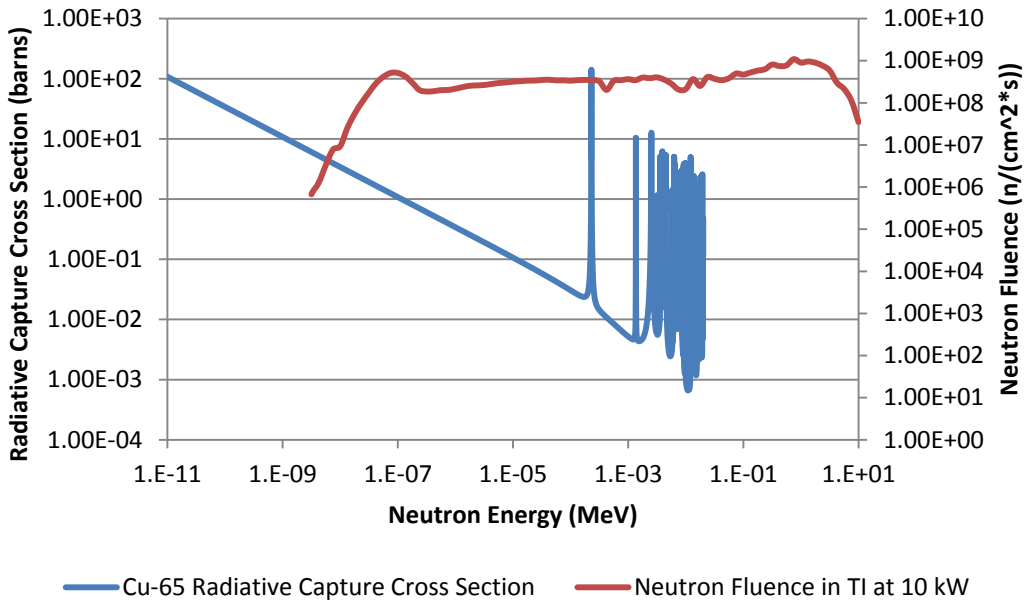

Figure 2.2. Microscopic cross section for ^{65}Cu and neutron fluence in University of Utah TRIGA reactor thermal irradiator port, cross section data source (9)

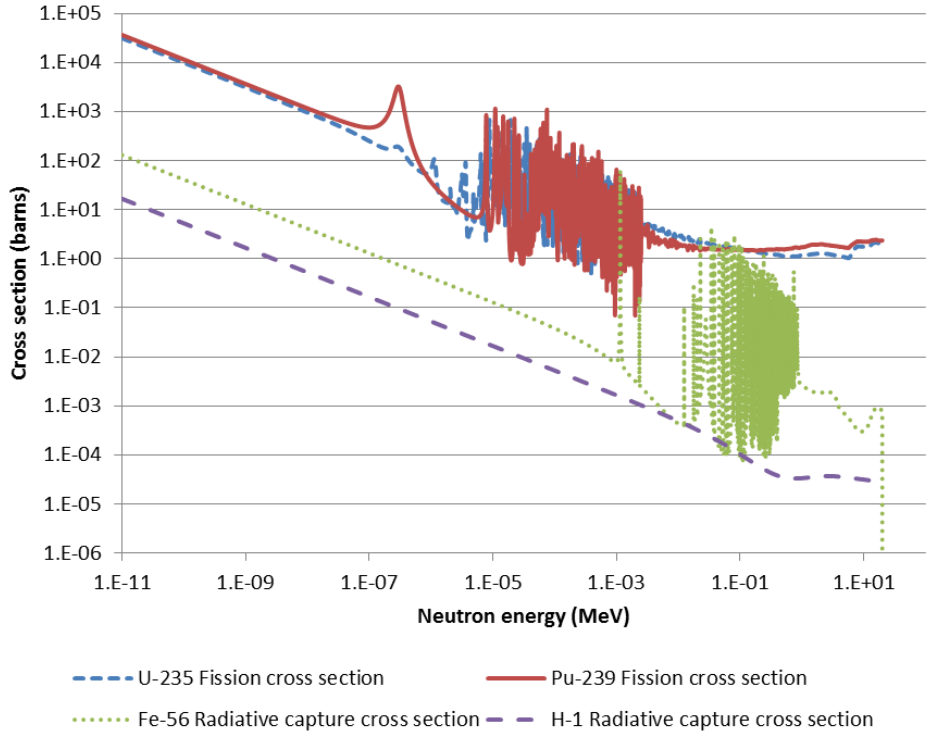

Figure 2.3. Microscopic cross sections for ^{235}U, ^{239}Pu, ^{56}Fe, and ^{1}H, data source (*9*)

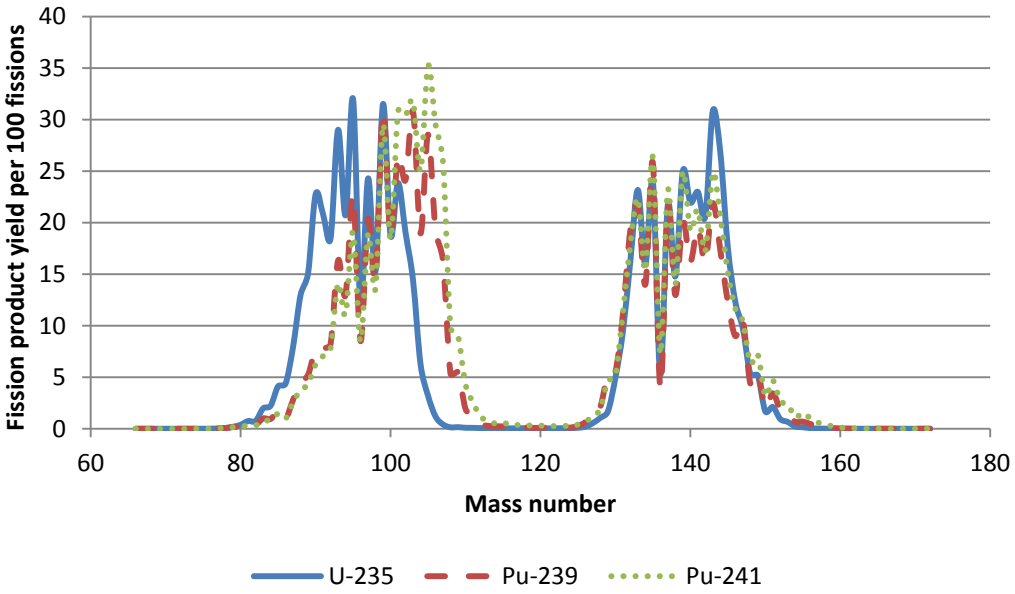

Figure 2.4. Distribution of fission products for thermal fission of ^{235}U, ^{239}Pu, ^{241}Pu, data source (*18*)

CHAPTER 3

PYTHON-BASED NEUTRON INTERACTION CALCULATOR: PyNIC

3.1. Introduction

As of May 2014, many neutron activation analysis precalculators exist *(19–22)* to perform rough estimates of activation products. Most of these calculators only take into account the thermal flux of a neutron beam, which is fully adequate to perform rough estimations. In order to achieve a higher level of accuracy though in neutron activation analysis and prompt gamma ray emissions from neutron capture, the entire neutron energy spectrum needs to be used. As it is presented the tool adds a benchmarked, higher level of accuracy for neutron activation analysis precalculations by calculating the activation across the entire neutron spectrum of a neutron source such as a reactor.

The Python-based neutron interaction calculator (PyNIC) is developed for its end use in the modeling of applications of compact neutron sources for applications in homeland security, nuclear power, and nuclear medicine. The majority of modeling for homeland security and nuclear power focused on the development of a simulation tool in Python that performs calculations on neutron activation and select inelastic and fission neutron interactions with a user-specified sample composition. The PyNIC was developed by using the neutron capture cross sections, select inelastic scattering cross sections, and

select fission cross sections in conjunction with the applicable equations to calculate the activation products or immediate gamma emissions. The PyNIC also includes the ability for the user to perform an MCNP simulation of the gamma spectrum a user would expect on an HPGe detector.

3.2. UUTR Irradiation Ports and MCNP6 Simulated Neutron Energy Spectrum

The UUTR has four commonly used irradiation ports. The four irradiation ports are the TI, the fast neutron irradiation facility (FNIF), the pneumatic irradiator (PI), and the central irradiator (CI). The neutron flux in each of these irradiation facilities was modeled using a complete MCNP6 model of the UUTR core. A plot of the neutron flux in all but the PI is shown in Fig. 3.1. Also, a complete flux profile for thermal neutrons and for fast neutrons is shown in Fig. 3.2 and Fig. 3.3, respectively. The highest total flux in the CI (7.4×10^{12} neutrons/(cm^2*s)) and the lowest is in the TI (7.3×10^{11} neutrons/(cm^2*s)). For calculations made in PyNIC, 2620 energy tally bins were used in MCNP6 with a F4:n tally from 1 cm below the centerline of the core to 1 cm above the centerline for each radiation port.

3.3. Radiative Capture, Inelastic Scattering, and Fission Cross Sections

The radiative capture, inelastic scattering, and fission cross sections from the Pointwise ENDF-VII at 300 K libraries were built into the PyNIC. These cross sections were downloaded from the atom.kaeri.re.kr website (*9*). The entire radiative capture cross section (all data points across the energy range for a given nuclide) for 243 nuclides

were built into the scripts. The reason for adding the complete cross section is that the activation can be calculated more accurately for a unique neutron beam energy spectrum and flux. The entire inelastic scattering or fission cross section was also built into the scripts for a few nuclides. Inelastic scattering cross sections were added for the first excitation state of C (natural abundance carbon) and the second, third, and fourth excitation levels of ^{16}O. Fission cross sections were added for ^{235}U, ^{238}U, and ^{239}Pu.

An example of the difference between using just the thermal cross section in the activation equation vs. the entire cross section is significant in the case of ^{66}Cu. As shown in the calculation in Eq. 3.2, the activity is 0.0062 mCi when just accounting for the neutrons with an energy from 0.0178 to 0.0237 eV while the PyNIC calculates an activity of 0.072 mCi when accounting for the entire neutron energy spectrum. In order to perform the calculations over the entire neutron energy spectrum of a given neutron beam, an algorithm was developed to process the cross section. This algorithm is described in Section 3.4.

3.4 Neutron Beam Energy Spectrum and Cross Section Library Processing

The PyNIC is capable of performing calculations for any neutron energy bin structure. An algorithm was added to the cross section library processing that uses the energy bin structure of the neutron beam to create a neutron cross section array with the same energy bin structure. This is done in order for the neutron activation equation to be solved for each individual energy bin associated with the neutron beam energy spectrum (take the integral over the whole spectrum as shown in Eq. 2.1). For example, if the

neutron beam energy bin structure has a neutron flux value between 1 eV and 10 eV (the upper energy value is used as the energy for that bin), the cross section for that energy bin is needed to perform the neutron activation calculation in Eq. 3.1. The ENDFVII cross section libraries that have been added to the PyNIC might have many cross section values between 1 eV and 10 eV though. Therefore, an algorithm searches for all the values in the cross section library for a given nuclide and averages them to give one single cross section value between 1 eV and 10 eV. This process is completed for every energy bin of the neutron beam so that the activation that occurs for each energy range can be calculated.

The algorithm for processing the cross section libraries adds great flexibility to the code because it allows a user to input a neutron energy spectrum with any energy bin structure. This can be very important because in many cases user input neutron spectrums will have far less energy resolution than the cross section libraries due either to poor energy resolution of neutron detectors or limitations on computation abilities. In the case of simulations done in MCNP to tally the neutron energy spectrum from a neutron source such as a reactor it is possible to create neutron tally structures with an energy resolution seen in cross section libraries, though it would be computationally expensive to achieve the level of error reduction needed. Also of note, the energy resolution for each nuclide in the ENDF libraries is not the same over every energy range. Therefore, the cross section library processing algorithm is necessary to process different nuclides.

3.5 Nuclear Decay Data for Radiative Capture

The gamma emissions from radiative capture can fall under two categories, the gamma rays emitted immediately after capture and those emitted from the radioactive daughter products. An example of gamma rays emitted immediately after capture would be neutron capture in hydrogen:

$$^{1}H + n \rightarrow {}^{2}H + \gamma \tag{3.3}$$

Neutron capture in ^{1}H does not lead to a radioactive daughter product but a gamma ray with the energy of 2223.3 keV is emitted during the capture process. An example of neutron capture leading to the production of a radioactive daughter product would be neutron capture in ^{65}Cu:

$$^{65}Cu + n \rightarrow {}^{66}Cu + \gamma \tag{3.4}$$

Neutron capture in ^{65}Cu leads not only to the immediate emission of gamma rays but also leads to the radioactive daughter product ^{66}Cu, which decays by beta emission with a half-life of 5.12 minutes. The beta decay of ^{66}Cu is also accompanied by the emission of gamma rays, as shown in Fig. 3.4, with the most frequently emitted gamma ray having an energy of 1039.2 keV.

In order to make a simulation tool that would be useful for active neutron interrogation and for neutron activation experiments, the immediate gamma emissions and the gamma emissions from radioactive daughter products were built into the PyNIC.

The radioactive decay data of the daughter products were pulled from the atom.kaeri.re.kr (*1*) website, while the immediate gamma emission data were taken from the IAEA Thermal Neutron Capture Gamma-rays webpage (*23*). The gamma emission rate for each radioactive daughter product can be calculated using Eq. 3.5 in conjunction with the known gamma emission rates per radioactive decay of the given nuclide. The instantaneous gamma emission rate while the sample is exposed to the neutron beam can be calculated using the gamma emission data for radiative capture in Eq. 3.5.

$$A_D(t) = \varphi(\sigma_p) m \left(\frac{N_A}{A_m}\right) A_{\%} \tag{3.5}$$

Every time the user selects a given nuclide, the PyNIC determines the activation and, if the data are available, calculates the immediate gamma emissions from radiative capture. The activation product is determined for all 238 nuclides built into the PyNIC, and the activity of each daughter product is determined if the daughter product is radioactive. The instantaneous gamma emissions are only calculated for the nuclides listed in Table 3.1.

3.6 Gamma Emissions from Inelastic Scattering and Fission

Gamma emissions from inelastic scattering are calculated each time the user selects C and ^{16}O in the user interface. The gamma emissions from inelastic scattering in other nuclides are not calculated. C and ^{16}O are included because their cross sections for inelastic scattering (2.51 mb for the first oxidation state of ^{16}O and 211 mb for ^{12}C at 14 MeV (*9*)) are much higher than the cross section for radiative capture (0.187 mb for ^{16}O

and 3.37 mb for ^{12}C at 0.025 eV) and because their signatures would be important in explosives detection using neutron interrogation. Other isotopes important in explosives detection have sufficient signatures from radiative capture and therefore do not have their inelastic scattering cross sections included in the PyNIC. The gamma emissions are assumed to be from ^{12}C and are for the first excitation level (4.43 MeV gamma rays) (*24*). The gamma emissions for O-16 are for the second, third, and fourth excitation levels (6.14, 6.91, 7.12 MeV gamma rays) (*24*). Gamma emissions from fission are calculated each time the user selects the ^{235}U, ^{238}U, and ^{239}Pu nuclides in the user interface. The gamma emissions for ^{235}U, ^{238}U, and ^{239}Pu were taken from simulations performed in MCNPX.

The MCNPX simulations performed were for a metal sphere (radius of 6.38 cm) of either ^{235}U, ^{238}U, or ^{239}Pu in a vacuum. A total of 2000 kcode cycles with 100000 particles per history were run. An F4:p (volume tally for x-rays/gamma rays) within the metal sphere was simulated and the results for each of the three isotopes is shown in Table 3.2. The results from the simulation are normalized to a per neutron basis. In order to enter the results in Table 3.2 into the PyNIC they needed to be normalized to a per fission basis; therefore, they were normalized based on an average neutron yield of 2.4355, 2.819, and 2.8836 (*25*) per fission event in ^{235}U, ^{238}U, and ^{239}Pu, respectively.

3.7 Sample Dose Rate Calculations

The sample dose rate at 1 foot is also calculated for NAA experiments. An NAA experiment at the University of Utah TRIGA (UUTR) facilities is performed by bringing the reactor up to a given power (typically between 1 kW and 90 kW), irradiating the

sample, removing the sample, and taking a dose rate measurement at 1 foot, and finally counting the activity of the radioactive daughter products on a HPGe detector. Before any NAA experiment, a calculation of the expected activity and dose rate from the sample at 1 foot is made. The dose rate calculations are performed to ensure that the dose rate experimenters will receive from the sample is below 1 mR/hr (limit in the UUTR facilities). The activity calculations are performed to ensure that the activity of the sample is high enough that the gamma emissions will be detectable on a HPGe detector. The dose is calculated for each sample component (and each gamma ray from that component) using (*26*):

$$Dose\ Rate\ \left(\frac{mrem}{hr}\right) = \frac{A_D(R)E(\frac{\mu}{\rho}) * (1.6 * 10^{-13})(1000)(3600)(10^5)}{4\pi r^2} \qquad (3.6)$$

A_D = activity of daughter isotope (Bq)

R = ratio of decays from a given isotope that emit a gamma ray of the given energy

E = decay energy for gamma ray (MeV)

μ/ρ = mass energy-absorption coefficient (cm^2/g)

r = distance from source (cm)

The PyNIC is used to compute the dose an experimenter would expect for a given set of experiment parameters so that the safe exposure rates are obtained. The key parameters that will ultimately determine the dose from the samples are sample mass, sample composition, irradiation time, decay time between the end of the irradiation and the time the sample is removed from shielding, and when adjustable, the neutron flux it is exposed to. In the instances where the dose rate the experimenter would experience is

too high, one or more of the experiment parameters can be adjusted to reduce the dose rate. An example of this dose calculation is shown below for the same experiment parameters used in Section 3.1 (0.05 g sample, 100% ^{65}Cu, 1 min irradiation time, 5 min decay time, TI port of UUTR TRIGA reactor at 10 kW). The activity calculated by the PyNIC is 0.072 mCi (2.66x10^6 Bq), the gamma emission at 1.0392 MeV is emitted 9.23% of the time, and the mass attenuation coefficient is 0.0625 cm^2/g.

$$Dose\ Rate$$

$$= \frac{2.66x10^6(0.0923)1.0392(0.0625) * (1.6 * 10^{-13})(1000)(3600)(10^5)}{4\pi 30.48^2}$$

$$= 0.0787 \frac{mrem}{hr} \tag{3.7}$$

As part of the dose rate calculation, mass energy-absorption coefficients have to be determined for each gamma ray. The mass energy-absorption coefficients in air from the NIST website (*27*) were built into the PyNIC, and an interpolation algorithm is used to determine the correct coefficient for a given gamma ray energy. Table 3.3 contains the data points from the NIST website.

To determine the correct coefficient, the algorithm first imports all of the decay gamma energies for the activated nuclide. It then determines which energy data points in Table 3.2 each gamma energy falls between (e.g., the 1.0392 MeV gamma ray from ^{66}Cu would fall between the 1 MeV and 1.25 MeV data points). The mass attenuation coefficients at 1 MeV and 1.25 MeV are 0.06358 cm^2/g and 0.05687 cm^2/g, respectively. Interpolation is then used to solve for the mass attenuation coefficient at 1.0392 MeV.

$$\frac{\mu}{\rho} = 0.06358 + (1.0392 - 1.00) * \frac{0.05687 - 0.06358}{1.25 - 1.00} = 0.0625 \frac{cm^2}{g} \tag{3.8}$$

This algorithm is used to solve for the mass attenuation factors at each gamma ray

energy.

3.8 Graphical User Interface

A graphical user interface (GUI), which is composed of Fig. 3.5 through Fig. 3.16, was developed to facilitate the use of the PyNIC. The GUI was built using the tkinter libraries included with a default install of Python. The GUI includes the following components:

1. An entry box for the sample mass (Fig. 3.5)
2. An entry box for the irradiation time (Fig. 3.6)
3. An entry box for the decay time between the neutron irradiation and when the sample is removed from shielding (Fig. 3.7)
4. A listbox for the different neutron beams (Fig. 3.8)
5. A total of five listboxes each containing 238 different isotopes for the user to select and a total of five entry boxes to input the percent abundance of each selected nuclide in the sample (Fig. 3.9)
6. A button (Fig. 3.10) that, when pressed, solves Eq. 3.1, Eq. 3.6, and Eq. 3.5 where applicable for each of the nuclides selected by the user. A report is also written to a text file and printed to the console (Fig. 3.11)
7. Entry box for the number histories to input to the MCNPX input file for the HPGe detector model (Fig. 3.12)
8. Entry box for the simulated count time in the HPGe detector model (Fig. 3.13)
9. Button to generate the MCNPX input file for the HPGe detector model (Fig. 3.14)
10. Button to run the MCNPX input file (Fig. 3.15)

11. Button to process the MCNPX output file after completion of the run (Fig. 3.16) After processing the output file, a report and a plot of the HPGe detector tally are also generated.

3.9 Values Reported By the PyNIC

The PyNIC generates a text file report (see Fig. 3.17) with the following values (the same values are also printed to the console):

- Instantaneous gamma ray emission rate from each selected nuclide from radiative capture
    - Top 5 gamma ray emissions for each nuclide
- Neutron activation products
    - Activity of activation products
    - Top 5 gamma emissions from each activation product
- Dose rate at 1 foot from sample (radiation protection for individuals handling sample)
- Instantaneous gamma ray emission rate from each selected nuclide from inelastic scattering
    - Top 5 gamma ray emissions for each nuclide
- Instantaneous gamma ray emission rate from each selected nuclide from fission
    - Top 5 gamma ray emissions for each nuclide

The report in Fig. 3.17 is generated by the PyNIC for the same experiment parameters used in previous examples with the exception of the sample being made out of pure ^{63}Cu instead of ^{65}Cu.

3.10 PyNIC Gamma Spectrum Simulator

An additional feature of the PyNIC is a gamma spectrum simulator. The gamma spectrum simulator uses MCNPX to model the gamma spectrum on a HPGe detector (model shown in Fig. 3.18) from either the instantaneous gamma rays or the activation products after a given period of time. This feature allows the user to visualize an idealized gamma spectrum that would be measured from the sample.

The MCNPX model consists of a high-purity germanium crystal with a radius of 3.355 cm and a height of 3.68 cm to model the spectrum. The crystal is located in a vacuum, and the gamma source is treated as a point source located 10 cm away from the top surface of the crystal as shown in Fig. 3.18. The energy spectrum of the gamma source is modeled as a ratio of either the instantaneous gamma emissions from the user selected nuclides or from the activation products. For example, if two nuclides are selected and the instantaneous gamma emission for the first is 1 MeV with an emission rate of 1000 gammas/sec and the second emits a gamma ray of 2 MeV with 3000 gammas/sec, the source would be modeled as a 1 MeV source being emitted 25% of the time and a 2 MeV source being emitted 75% of the time.

The energy bin configuration of the gamma ray tally in the Ge crystal goes from 1 keV to 1.5 MeV with 0.3659 keV energy bins. A plot of the spectrum is generated on completion of the MCNPX simulation using the Matplotlib library (*28*) in Python. An example of this plot is shown in Fig. 3.19. The number of counts are based on the activity of the sample. A complete flow sheet-data of the PyNIC is shown in Fig. 3.20.

3.11 Assumptions in PyNIC Calculations

A number of key assumptions are made in the calculations in the PyNIC. The following are the key assumptions made:

- The neutron energy spectrum is assumed to be uniform throughout the entire sample and there is no accounting for the collision angle of the neutron with the nucleus
- When the daughter product of neutron capture decays to another radioactive nuclide, this second nuclide is ignored
- The gamma emissions from fission are only prompt gamma rays

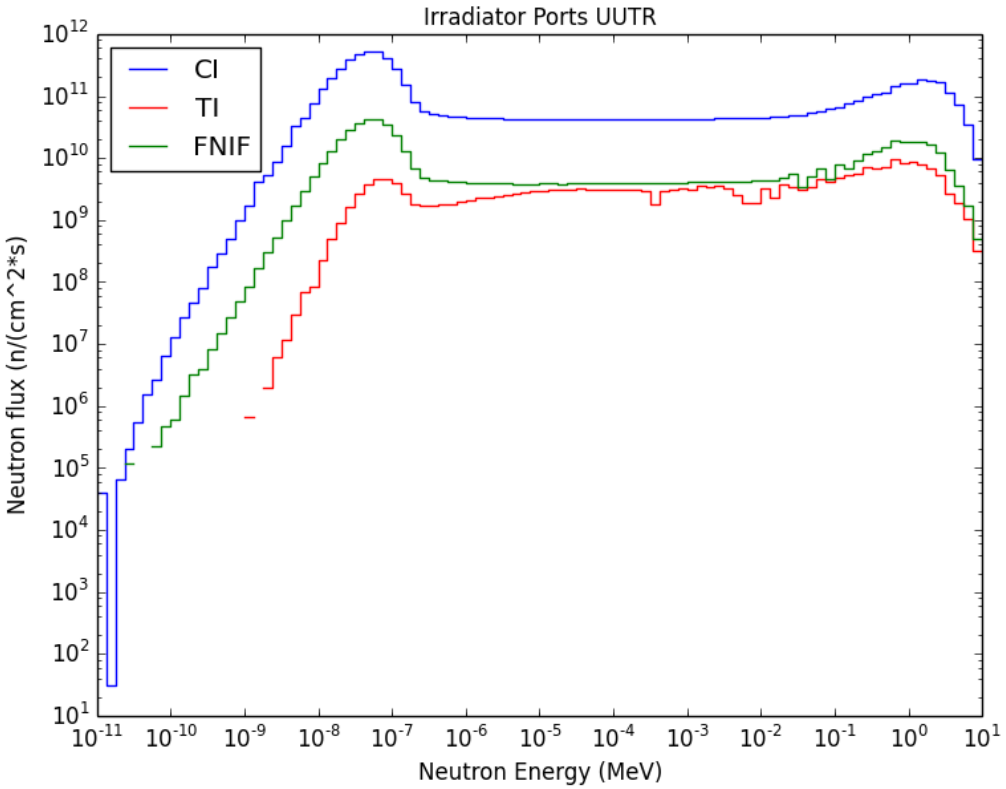

Figure 3.1. Flux plot of the UUTR CI, TI, and FNIF. Simulated in MCNP6.

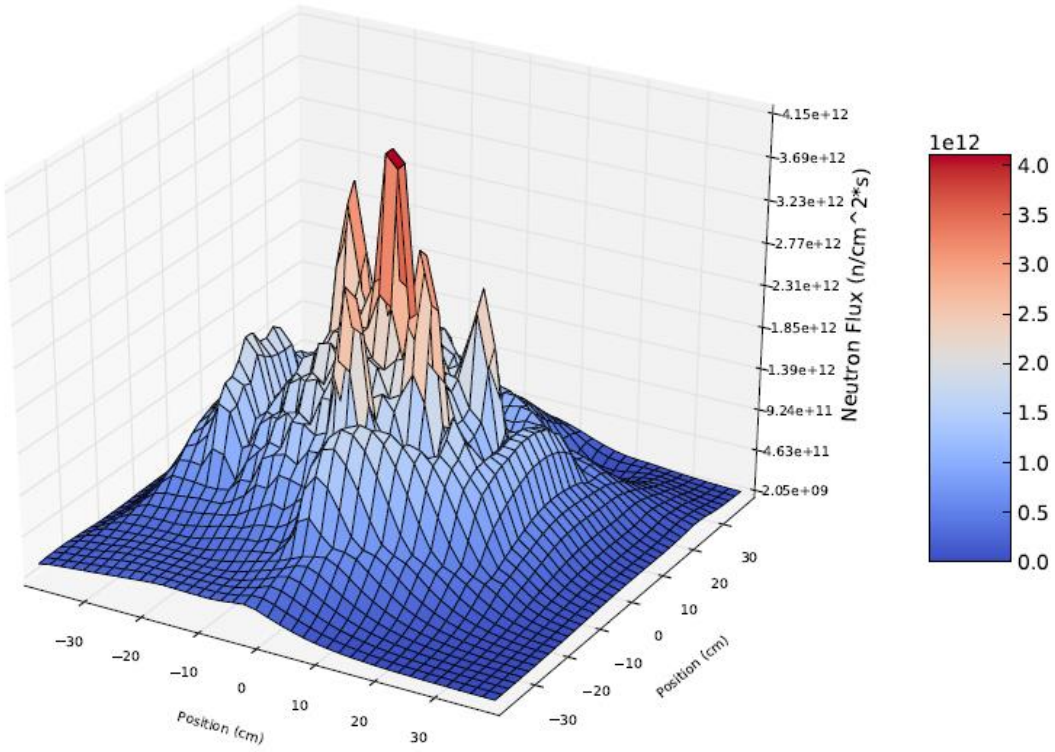

Figure 3.2. 3D thermal neutron flux across UUTR core and irradiation facilities. Simulated in MCNP6

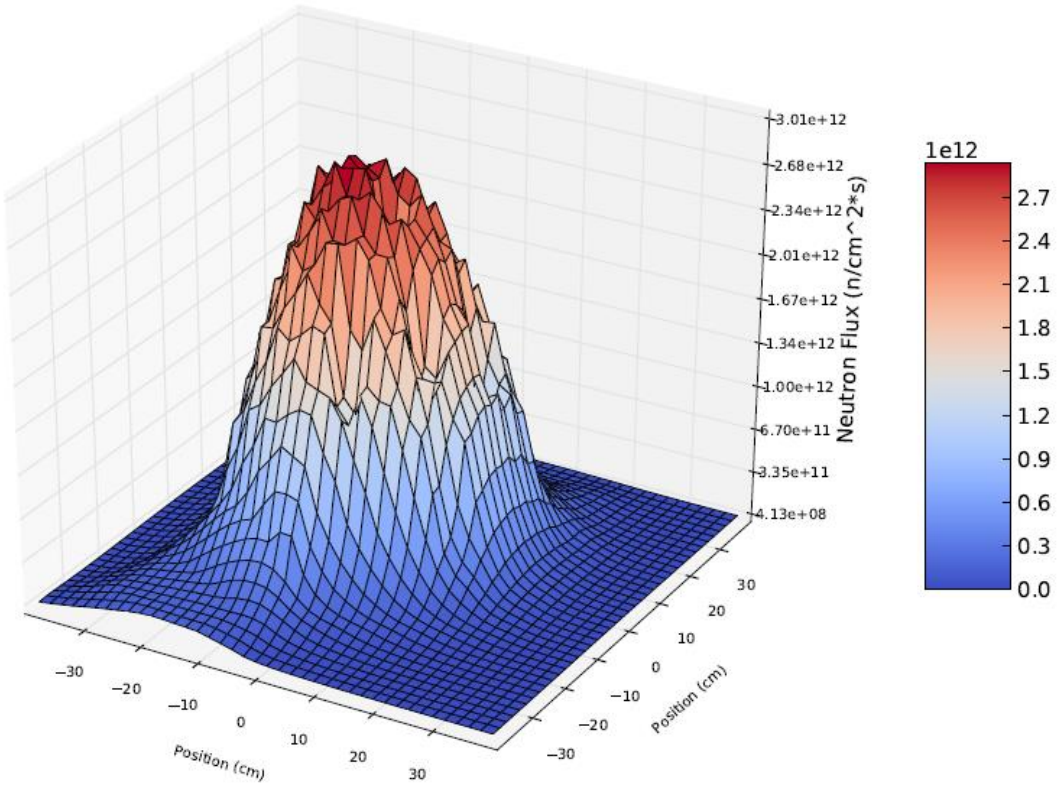

Figure 3.3. 3D fast neutron flux across UUTR core and irradiation facilities. Simulated in MCNP6.

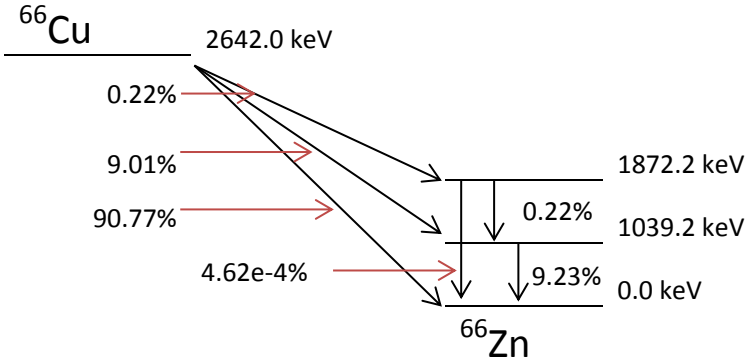

Figure 3.4. ^{66}Cu β^- decay scheme, data source (*9*)

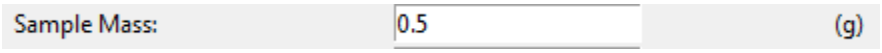

Figure 3.5. Sample mass entry box

Figure 3.6. Irradiation time entry box

Figure 3.7. Decay time entry box

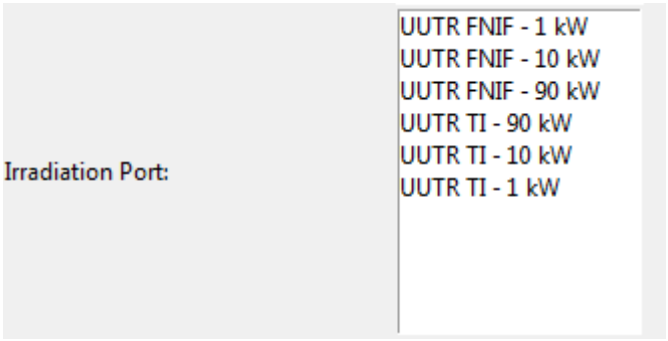

Figure 3.8. PyNIC: Listbox of neutron beams

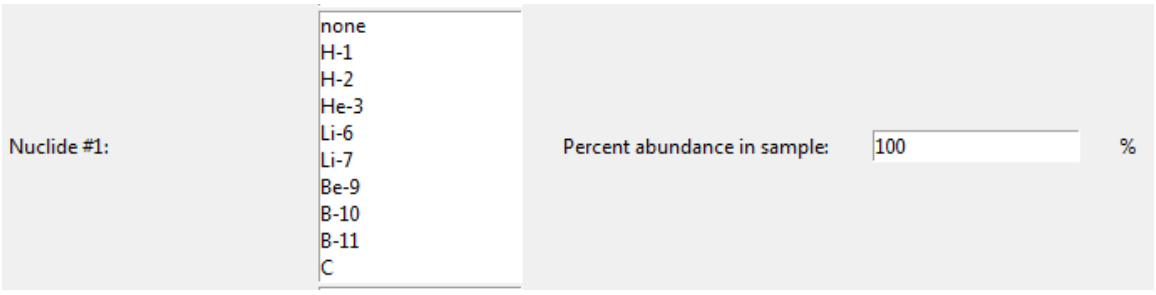

Figure 3.9. PyNIC: Nuclide #1 listbox and percent abundance listbox

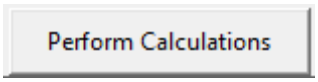

Figure 3.10. PyNIC: Button to perform calculations based on user input

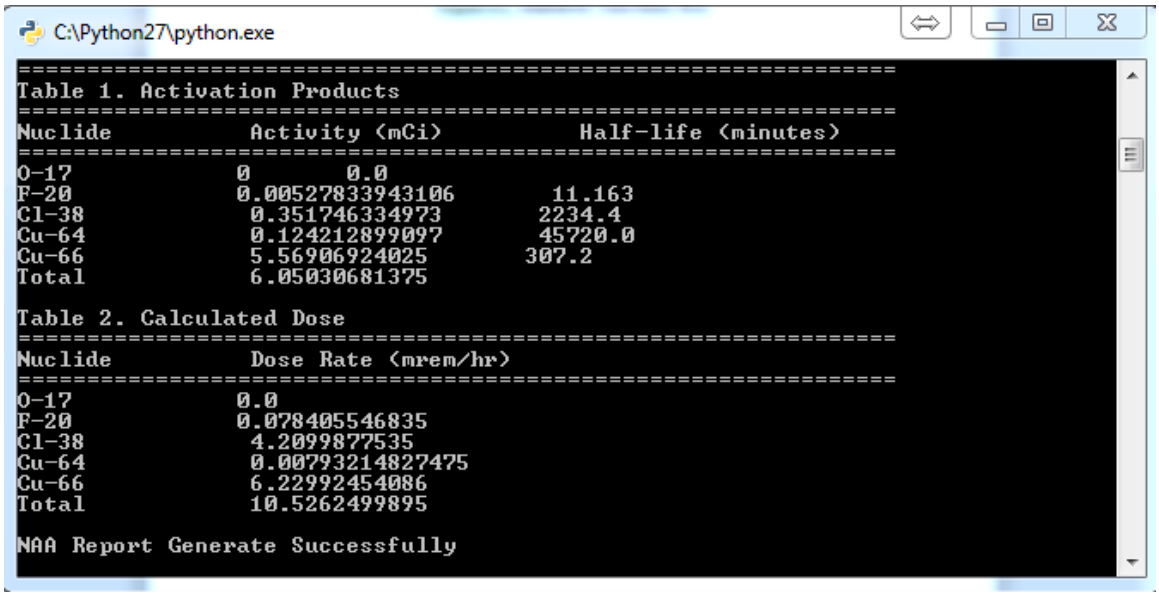

Figure 3.11. PyNIC: Console after report is generated

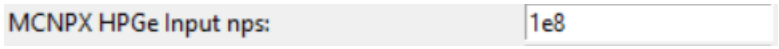

Figure 3.12. PyNIC: Entry box for number of gamma histories to run in MCNPX simulation

Figure 3.13. PyNIC: Entry box for HPGe count time

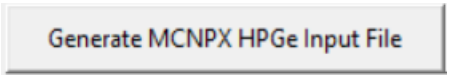

Figure 3.14. PyNIC: Button to generate MCNPX HPGe input file

Figure 3.15. PyNIC: Button to run MCNPX HPGe input file

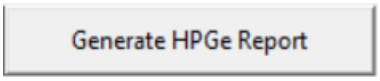

Figure 3.16. PyNIC: Button to process MCNPX HPGe output file

==========
PyNIC Version 1.01B 5-May-2014
==========
Table 1. Activation Products
==========

Nuclide	Activity (mCi)	Half-life (minutes)
Cu-64	0.00215	762
none	NA	NA
none	NA	NA
none	NA	NA
none	NA	NA
Total	0.00215	

Table 2. Calculated Dose at 1 ft
==========

Nuclide	Dose Rate (mrem/hr)
Cu-64	0.000137613467962
none	0.0
none	0.0
none	0.0
none	0.0
Total	0.000137613467962

Table 3. Gamma Emissions from Cu-64
==========

Gamma Energy (MeV)	Decay Ratio (per radioactive decay of Cu-64)
1.35	0.00473

==========
Table 4. Neutron Capture Rate for Selected Neutron Beam
==========

Nuclide	Neutron Captures per Second
Cu-64	8.81e07
none	NA
none	NA
none	NA
none	NA
Total	8.81e07

Table 5. Instantaneous Gamma Emissions from Cu-63

Figure 3.17. PyNIC report on: activity, dose, and gamma ray emissions

Gamma Energy (MeV)	Decay Ratio (per neutron capture in Cu-63)
7.92	0.331
0.278	0.240
7.64	0.162
0.159	0.150
7.31	0.0896

Figure 3.17.Continued

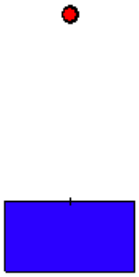

Figure 3.18. MCNPX model of a germanium crystal for simulating detector response 10 cm from a point source

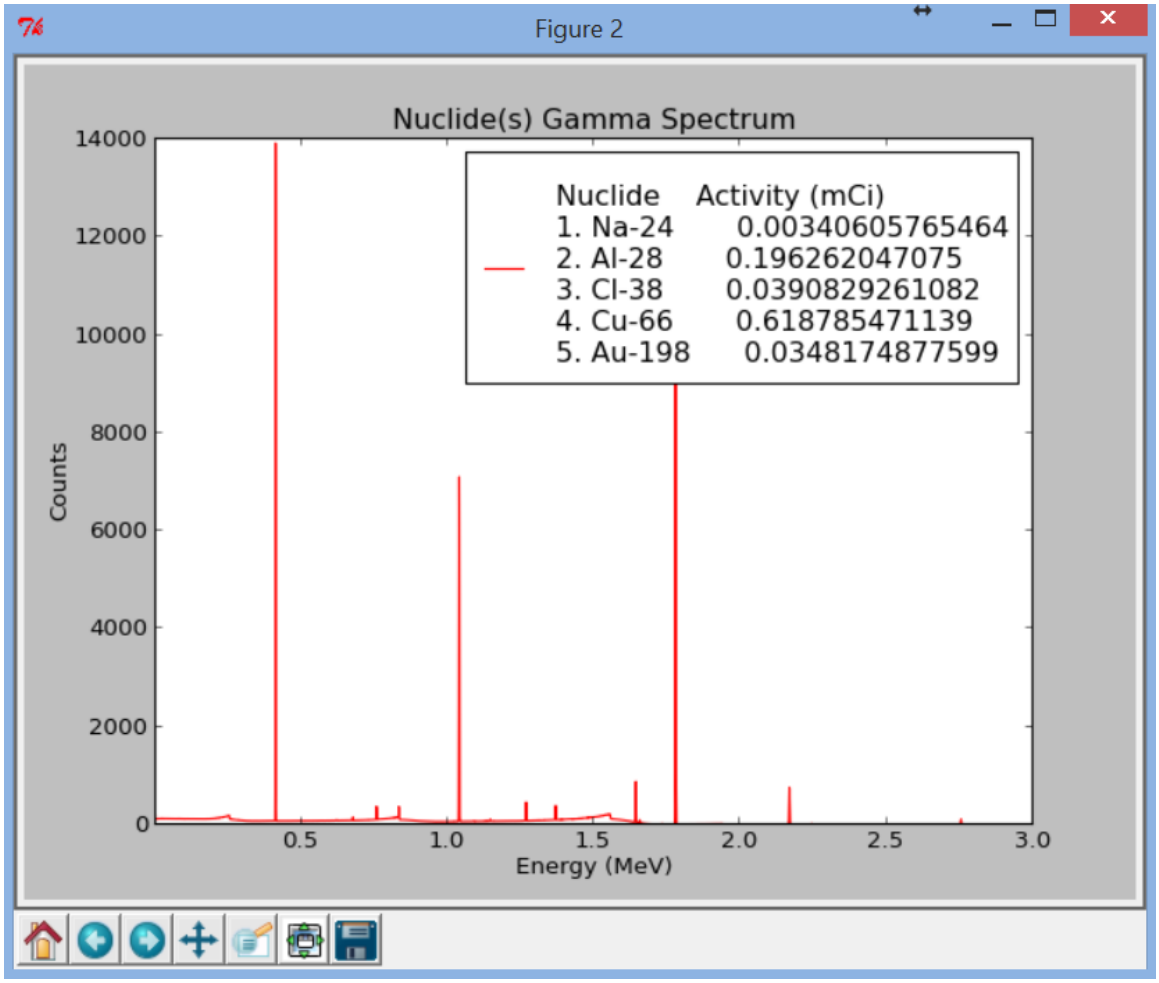

Figure 3.19. Plot of HPGe gamma spectrum as simulated in MCNPX

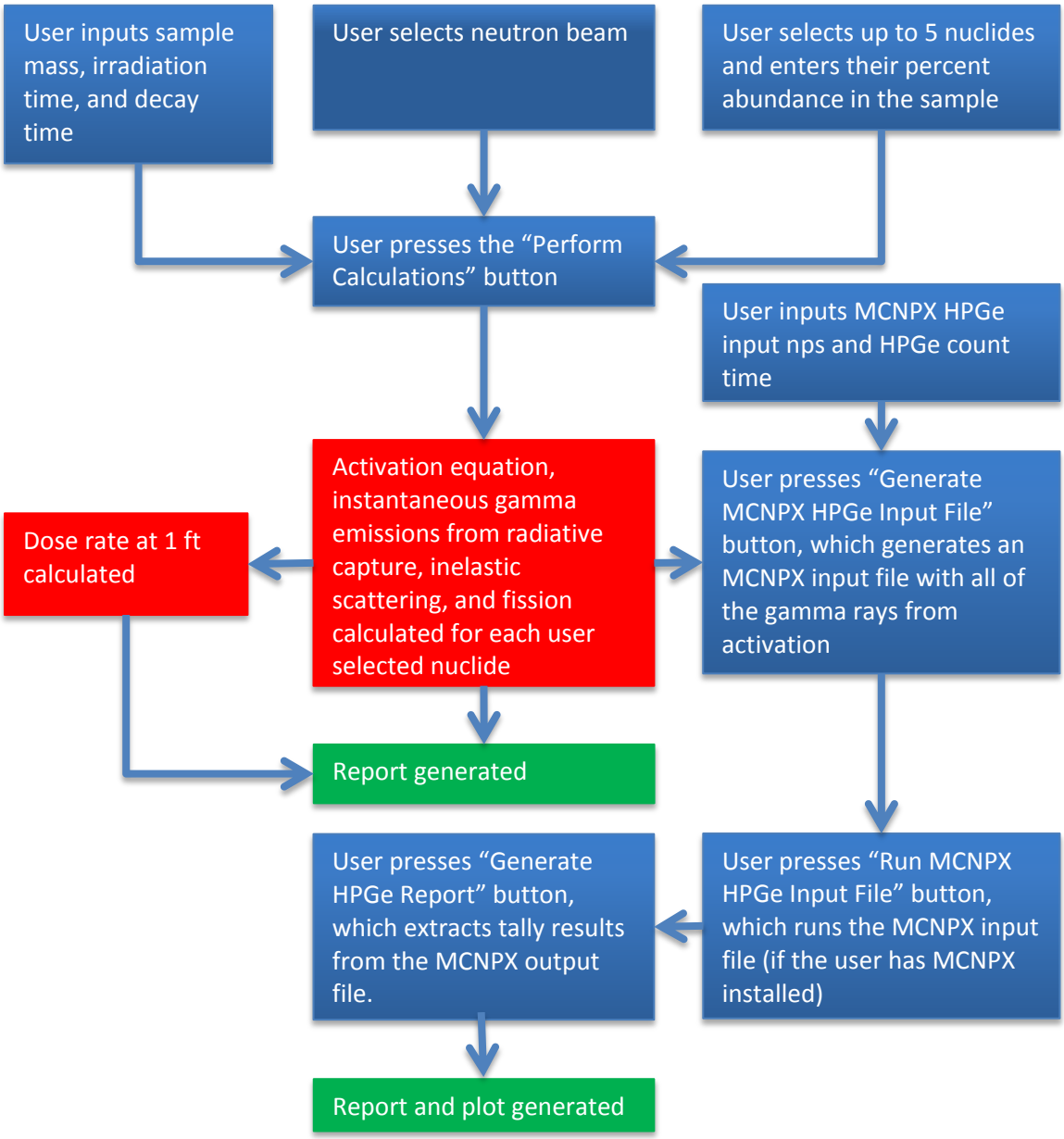

Figure 3.20. Flow chart of PyNIC

Table 3.1. Nuclides in the PyNIC with instantaneous gamma ray emission data

^{1}H	^{2}H	^{6}Li	^{7}Li	^{9}Be	^{12}C	^{14}N	^{16}O	^{19}F	^{23}Na
^{24}Mg	^{25}Mg	^{26}Mg	^{27}Al	^{28}Si	^{29}Si	^{30}Si	^{31}P	^{32}S	^{33}S
^{34}S	^{36}S	^{35}Cl	^{37}Cl	^{36}Ar	^{40}Ar	^{39}K	^{40}K	^{41}K	^{40}Ca
^{42}Ca	^{43}Ca	^{48}Ca	^{45}Sc	^{47}Ti	^{48}Ti	^{49}Ti	^{50}Ti	^{50}Cr	^{52}Cr
^{55}Mn	^{56}Fe	^{58}Fe	^{58}Ni	^{59}Ni	^{60}Ni	^{61}Ni	^{62}Ni	^{64}Ni	^{63}Cu
^{127}I	^{129}Xe	^{182}W	^{183}W	^{184}W	^{197}Au	^{230}Th	^{232}Th	^{235}U	^{238}U
^{239}Pu									

Table 3.2. F4:p tally results and associated error from MCNPX simulations of metal ^{235}U, ^{238}U, and ^{239}Pu spheres

E (MeV)	Pu-239 (Metal)		U-235 (Metal)		U-238 (Metal)	
	F4:p	SEM	F4:p	SEM	F4:p	SEM
1.00E-01	3.62E-05	0.0001	6.20E-05	0.0001	2.94E-05	0.0001
2.00E-01	8.45E-05	0.0001	3.74E-05	0.0001	1.91E-05	0.0002
3.00E-01	5.86E-05	0.0002	5.07E-05	0.0002	2.55E-05	0.0002
4.00E-01	9.45E-05	0.0002	8.82E-05	0.0002	3.90E-05	0.0002
5.00E-01	1.27E-04	0.0002	1.15E-04	0.0002	4.85E-05	0.0003
6.00E-01	2.10E-04	0.0002	1.83E-04	0.0002	6.89E-05	0.0003
7.00E-01	1.51E-04	0.0002	1.41E-04	0.0002	5.33E-05	0.0003
8.00E-01	1.44E-04	0.0002	1.33E-04	0.0002	4.78E-05	0.0004
9.00E-01	1.31E-04	0.0003	1.18E-04	0.0003	4.34E-05	0.0004
1.00E+00	1.18E-04	0.0003	1.14E-04	0.0003	4.05E-05	0.0005
1.10E+00	1.07E-04	0.0003	9.22E-05	0.0003	3.30E-05	0.0006
1.20E+00	9.90E-05	0.0004	9.05E-05	0.0004	3.11E-05	0.0006
1.30E+00	8.95E-05	0.0004	8.91E-05	0.0004	2.70E-05	0.0007
1.40E+00	7.89E-05	0.0004	8.51E-05	0.0004	2.32E-05	0.0007
1.50E+00	6.80E-05	0.0005	7.98E-05	0.0004	2.17E-05	0.0008
1.60E+00	5.96E-05	0.0005	5.43E-05	0.0005	1.80E-05	0.0008
1.70E+00	5.31E-05	0.0006	5.07E-05	0.0005	1.70E-05	0.0009
1.80E+00	4.71E-05	0.0006	4.71E-05	0.0005	1.51E-05	0.0009
1.90E+00	4.23E-05	0.0006	4.48E-05	0.0006	1.34E-05	0.001
2.00E+00	3.82E-05	0.0007	4.26E-05	0.0006	1.25E-05	0.001
2.10E+00	3.47E-05	0.0007	2.99E-05	0.0007	1.11E-05	0.0011
2.20E+00	3.16E-05	0.0008	2.86E-05	0.0007	1.02E-05	0.0011
2.30E+00	2.86E-05	0.0008	2.73E-05	0.0007	8.70E-06	0.0012
2.40E+00	2.61E-05	0.0008	2.62E-05	0.0008	7.29E-06	0.0014
2.50E+00	2.37E-05	0.0009	2.52E-05	0.0008	6.67E-06	0.0014
2.60E+00	2.14E-05	0.0009	1.75E-05	0.0009	5.82E-06	0.0015
2.70E+00	1.94E-05	0.001	1.65E-05	0.0009	5.45E-06	0.0016
2.80E+00	1.74E-05	0.001	1.56E-05	0.001	4.67E-06	0.0017
2.90E+00	1.57E-05	0.0011	1.48E-05	0.001	3.93E-06	0.0019
3.00E+00	1.40E-05	0.0011	1.41E-05	0.001	3.59E-06	0.002
3.10E+00	1.25E-05	0.0012	9.60E-06	0.0012	3.02E-06	0.0021
3.20E+00	1.12E-05	0.0013	8.97E-06	0.0013	2.77E-06	0.0023
3.30E+00	1.00E-05	0.0014	8.37E-06	0.0013	2.34E-06	0.0025
3.40E+00	9.13E-06	0.0014	7.96E-06	0.0014	1.92E-06	0.0027
3.50E+00	8.24E-06	0.0015	7.56E-06	0.0014	1.75E-06	0.0029
3.60E+00	7.50E-06	0.0016	5.59E-06	0.0016	1.48E-06	0.003
3.70E+00	6.84E-06	0.0016	5.30E-06	0.0017	1.52E-06	0.003
3.80E+00	6.20E-06	0.0017	5.04E-06	0.0017	9.75E-07	0.0038

Table 3.2. Continued

E (MeV)	Pu-239 (Metal)		U-235 (Metal)		U-238 (Metal)	
	F4:p	SEM	F4:p	SEM	F4:p	SEM
3.90E+00	5.68E-06	0.0018	4.80E-06	0.0018	7.65E-07	0.0042
4.00E+00	5.18E-06	0.0019	4.58E-06	0.0018	1.10E-06	0.0034
4.10E+00	4.74E-06	0.002	3.22E-06	0.0021	1.74E-06	0.0026
4.20E+00	4.29E-06	0.0021	3.02E-06	0.0022	1.20E-06	0.0032
4.30E+00	3.90E-06	0.0022	2.84E-06	0.0022	4.87E-07	0.0054
4.40E+00	3.55E-06	0.0023	2.64E-06	0.0023	3.95E-07	0.0062
4.50E+00	3.20E-06	0.0024	2.47E-06	0.0024	3.79E-07	0.0063
4.60E+00	2.92E-06	0.0025	1.67E-06	0.0029	3.40E-07	0.0067
4.70E+00	2.66E-06	0.0026	1.55E-06	0.003	3.55E-07	0.0065
4.80E+00	2.45E-06	0.0027	1.46E-06	0.0031	3.19E-07	0.0069
4.90E+00	2.21E-06	0.0028	1.40E-06	0.0032	2.94E-07	0.0073
5.00E+00	2.02E-06	0.003	1.35E-06	0.0032	2.89E-07	0.0074
5.10E+00	1.84E-06	0.0031	1.15E-06	0.0034	1.81E-07	0.0093
5.20E+00	1.70E-06	0.0032	1.15E-06	0.0034	1.79E-07	0.0093
5.30E+00	1.56E-06	0.0034	1.15E-06	0.0034	1.54E-07	0.01
5.40E+00	1.43E-06	0.0035	1.14E-06	0.0034	1.27E-07	0.011
5.50E+00	1.30E-06	0.0037	1.11E-06	0.0035	1.25E-07	0.0111
5.60E+00	1.18E-06	0.0038	9.42E-07	0.0037	9.04E-08	0.0132
5.70E+00	1.09E-06	0.004	8.69E-07	0.0038	8.74E-08	0.0131
5.80E+00	9.96E-07	0.0042	7.88E-07	0.004	7.13E-08	0.0146
5.90E+00	9.00E-07	0.0044	7.21E-07	0.0043	5.21E-08	0.0169
6.00E+00	8.03E-07	0.0046	6.56E-07	0.0045	5.43E-08	0.0168
6.10E+00	7.12E-07	0.0049	3.71E-07	0.0055	3.49E-08	0.0206
6.20E+00	6.40E-07	0.0052	3.25E-07	0.0059	3.52E-08	0.0204
6.30E+00	5.73E-07	0.0055	2.88E-07	0.0062	3.62E-08	0.0209
6.40E+00	5.12E-07	0.0059	2.50E-07	0.0067	3.57E-08	0.0208
6.50E+00	4.50E-07	0.0063	2.15E-07	0.0072	3.49E-08	0.0207
6.60E+00	3.97E-07	0.0067	1.86E-07	0.0078	3.55E-08	0.0205
6.70E+00	3.62E-07	0.0071	1.59E-07	0.0084	3.48E-08	0.0207
6.80E+00	3.22E-07	0.0075	1.38E-07	0.009	3.42E-08	0.021
6.90E+00	2.85E-07	0.0079	1.18E-07	0.0096	3.50E-08	0.0206
7.00E+00	2.55E-07	0.0084	1.04E-07	0.0103	3.32E-08	0.0212
7.10E+00	2.26E-07	0.0088	9.04E-08	0.011	3.29E-08	0.0209
7.20E+00	2.02E-07	0.0095	7.93E-08	0.0117	3.36E-08	0.0209
7.30E+00	1.78E-07	0.01	6.91E-08	0.0125	1.59E-08	0.0301
7.40E+00	1.55E-07	0.0108	5.65E-08	0.0138	0.00E+00	0
7.50E+00	1.29E-07	0.0116	4.69E-08	0.015	0.00E+00	0
7.60E+00	1.05E-07	0.0128	3.56E-08	0.0172	0.00E+00	0
7.70E+00	8.64E-08	0.0142	2.51E-08	0.0207	0.00E+00	0
7.80E+00	6.62E-08	0.0162	1.27E-08	0.0291	0.00E+00	0

Table 3.2. Continued

E (MeV)	Pu-239 (Metal)		U-235 (Metal)		U-238 (Metal)	
	F4:p	SEM	F4:p	SEM	F4:p	SEM
7.90E+00	4.36E-08	0.0191	7.92E-09	0.0365	0.00E+00	0
8.00E+00	2.35E-08	0.0247	3.42E-09	0.0556	0.00E+00	0
8.10E+00	1.24E-08	0.0319	5.21E-10	0.1527	0.00E+00	0
8.20E+00	0.00E+00	0	0.00E+00	0	0.00E+00	0
8.30E+00	0.00E+00	0	0.00E+00	0	0.00E+00	0
8.40E+00	0.00E+00	0	0.00E+00	0	0.00E+00	0
8.50E+00	0.00E+00	0	0.00E+00	0	0.00E+00	0
8.60E+00	0.00E+00	0	0.00E+00	0	0.00E+00	0
8.70E+00	0.00E+00	0	0.00E+00	0	0.00E+00	0
8.80E+00	0.00E+00	0	0.00E+00	0	0.00E+00	0
8.90E+00	0.00E+00	0	0.00E+00	0	0.00E+00	0
9.00E+00	0.00E+00	0	0.00E+00	0	0.00E+00	0
9.10E+00	0.00E+00	0	0.00E+00	0	0.00E+00	0
9.20E+00	0.00E+00	0	0.00E+00	0	0.00E+00	0
9.30E+00	0.00E+00	0	0.00E+00	0	0.00E+00	0
9.40E+00	0.00E+00	0	0.00E+00	0	0.00E+00	0
9.50E+00	0.00E+00	0	0.00E+00	0	0.00E+00	0
9.60E+00	0.00E+00	0	0.00E+00	0	0.00E+00	0
9.70E+00	0.00E+00	0	0.00E+00	0	0.00E+00	0
9.80E+00	0.00E+00	0	0.00E+00	0	0.00E+00	0
9.90E+00	0.00E+00	0	0.00E+00	0	0.00E+00	0
1.00E+01	0.00E+00	0	0.00E+00	0	0.00E+00	0

Table 3.3. Mass attenuation coefficients for dry air (near sea level), data source (*27*)

Energy (MeV)	**μ/ρ (cm^2/g)**
1.00E-03	3.61E+03
1.50E-03	1.19E+03
2.00E-03	5.28E+02
3.00E-03	1.63E+02
3.20E-03	1.34E+02
3.20E-03	1.49E+02
4.00E-03	7.79E+01
5.00E-03	4.03E+01
6.00E-03	2.34E+01
8.00E-03	9.92E+00
1.00E-02	5.12E+00
1.50E-02	1.61E+00
2.00E-02	7.78E-01
3.00E-02	3.54E-01
4.00E-02	2.49E-01
5.00E-02	2.08E-01
6.00E-02	1.88E-01
8.00E-02	1.66E-01
1.00E-01	1.54E-01
1.50E-01	1.36E-01
2.00E-01	1.23E-01
3.00E-01	1.07E-01
4.00E-01	9.55E-02
5.00E-01	8.71E-02
6.00E-01	8.06E-02
8.00E-01	7.07E-02
1.00E+00	6.36E-02
1.25E+00	5.69E-02
1.50E+00	5.18E-02
2.00E+00	4.45E-02
3.00E+00	3.58E-02
4.00E+00	3.08E-02
5.00E+00	2.75E-02
6.00E+00	2.52E-02
8.00E+00	2.23E-02
1.00E+01	2.05E-02
1.50E+01	1.81E-02
2.00E+01	1.71E-02

CHAPTER 4

COMPARISON OF PyNIC NEUTRON ACTIVATION CALCULATIONS TO EXPERIMENTS PERFORMED IN THE UNIVERSITY OF UTAH TRIGA REACTOR

4.1. Experiment Setup

A series of irradiation experiments in the UUTR were performed for a comparison to activation calculations made in the PyNIC. The experiment involved irradiating nickel wire samples in the (TI) of the UUTR across multiple reactor power levels. The irradiation parameters for each irradiation are listed in Table 4.1. Coal fly ash standards (1633c) (*29*) from the National Institute of Standards and Technology (NIST) were used in the second experiment as further validation of the calculator. These samples were also irradiated in the thermal irradiator of the UUTR. The irradiations performed are listed in Table 4.2.

4.2 Experiment Results

Table 4.3 contains the results of the nickel irradiation experiments. The activity of the irradiated sample was measured using a HPGe detector, and the ^{65}Ni was identified using the GENIE software. A high purity germanium detector was used to count the sample because of the high gamma ray energy resolution achievable compared to NaI or

$LaBr_3$ detectors. The sample was placed on the detector inside of a lead and copper shield (See Fig. 4.1). The ^{65}Ni was analyzed because it has the highest activity of any of the activation products in naturally abundant nickel. A plot of sample activity (measured and predicted) is shown in Fig. 4.2, which shows a very good agreement between measured and predicted values across the power range from one to ninety kW. The average percent difference between the estimate and the measured values is 4.01%. All samples were within +/- 10% except for an irradiation at 1 kW (10.86%) and one at 10 kW (18.43%). Also, the percent difference for the estimated activity of all samples (with the exception of the sample with a 18.43%) fell within the +/- calculated by the GENIE software.

The irradiation results for the NIST coal fly ash are given in Tables 4.4, 4.5, and 4.6. The samples were counted using the same detector as the nickel wire samples, with the exception of a couple samples that were counted using another HPGe detector. While the coal fly ash has many nuclides present, the only nuclides analyzed in this work were ^{56}Mn, ^{40}K, and ^{139}Ba. A plot of sample activity (measured and predicted) for each nuclide is shown in Fig. 4.3, 4.4, and 4.5, which shows a very good agreement between measured and predicted values across the power range from 1 to 90 kW with the exception of the irradiations at 70 kW for ^{139}Ba. The average percent difference between the estimate and the measured values for ^{56}Mn, ^{40}K, and ^{139}Ba is 23.74%, 37.75%, and 21.86%, respectively. The removal of three samples with the greatest error decreases the percent difference for ^{40}K to 17.40%. Also of note, the ^{40}K and ^{139}Ba had high relative errors reported by the GENIE software, likely due to relatively short count times (10 minutes). Longer irradiation times, coupled with longer decay times to remove short-lived nuclide

interference would help to improve counting statistics for ^{40}K.

The accuracy of the PyNIC in calculating the dose expected from the sample is good for samples, though the accuracy is not to same level as activity predictions. This is due partly that calculator does not take into account any contaminates or unaccounted for nuclides in the sample or any contaminates on the container or vial. Also, the handheld dose meter does not have the same level of accuracy with regards to dose as a HPGe does with activity. And finally, the user holding the dose meter is not going to consistently hold the meter exactly 1 foot from the source. The dose results for the nickel irradiations are shown in Table 4.7, and the dose results for the NIST irradiations is shown in Table 4.8. The nickel samples at each power were irradiated together so there are only six dose values. The simulated dose values do give good estimates to help plan safe NAA experiments.

Discrepancies between measured and predicted values occur because of a number of factors. The first is the calibration performed on the germanium detectors. The source used has too high of activity for the counting geometries used. Also, better implementation of NAA experimental techniques and counting techniques will lead to more accurate measured activities. Improvements to the cross section processing algorithm in PyNIC are also needed. These improvements will likely lead to better agreement between measured and simulated values.

The performance of PyNIC in calculating the activity of daughter products compared to actual measurements shows its usefulness in predicting nuclear signatures. While not tested through actual experiments, the same level of accuracy is expected for prompt gamma emissions from neutron capture. The tool allows for the user to accurately

simulate activation products for a sample, thereby lending its value to a wide variety of fields within nuclear power, nuclear medicine, and homeland security applications.

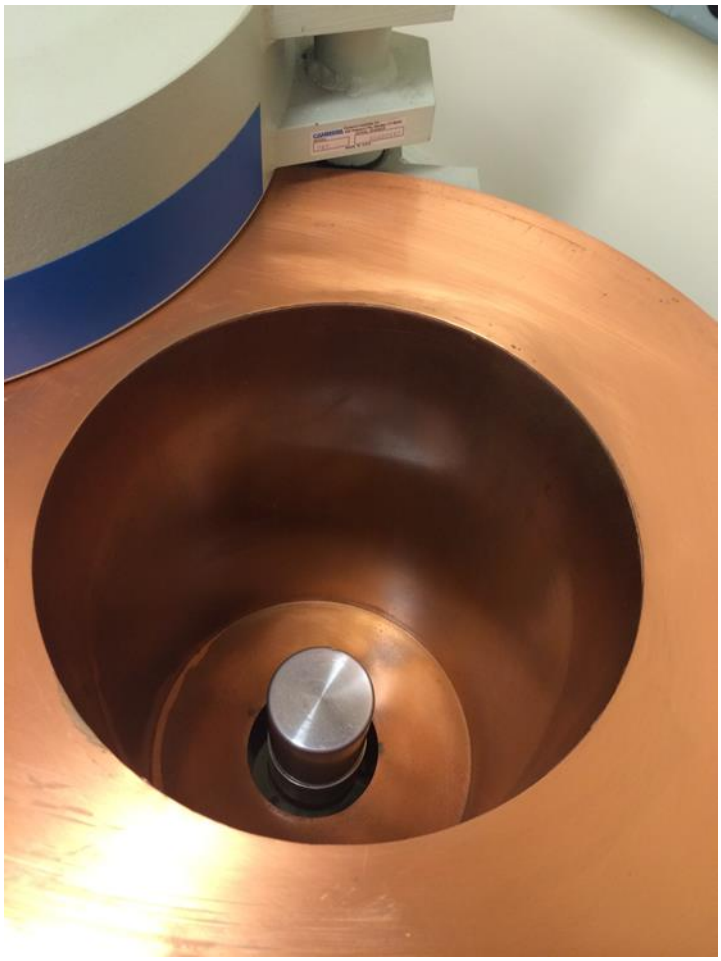

Figure 4.1. HPGe detector with Canberra lead and copper shielding

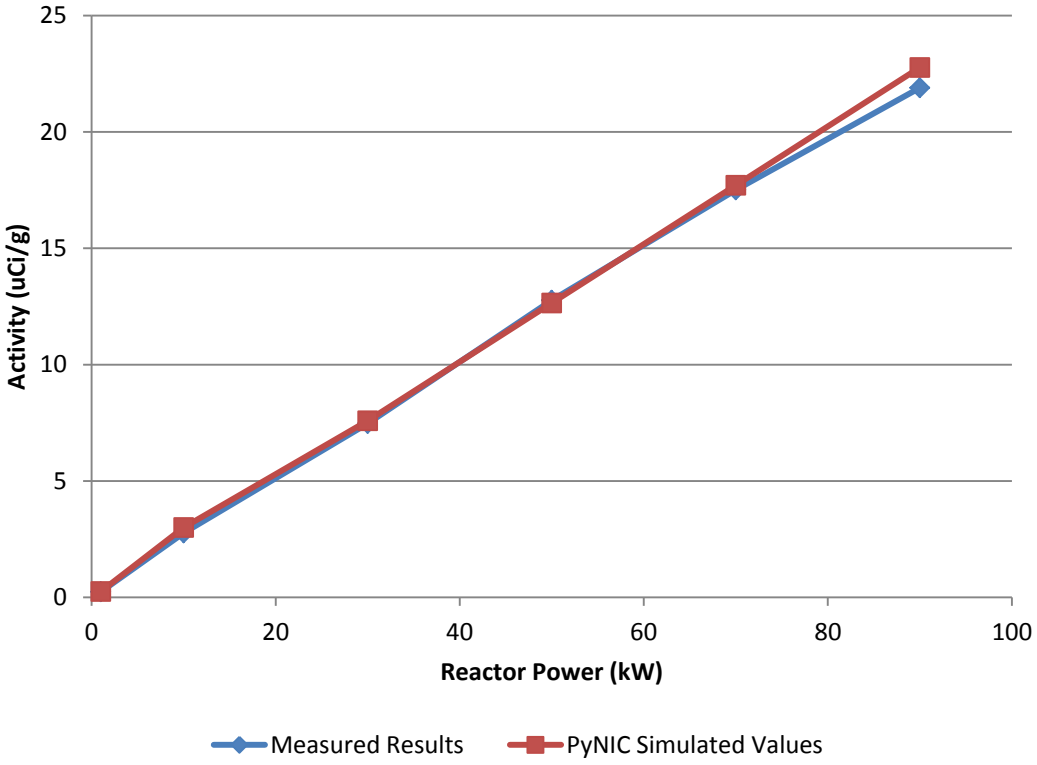

Figure 4.2. Measured nickel irradiation results and PyNIC simulated values vs. reactor power

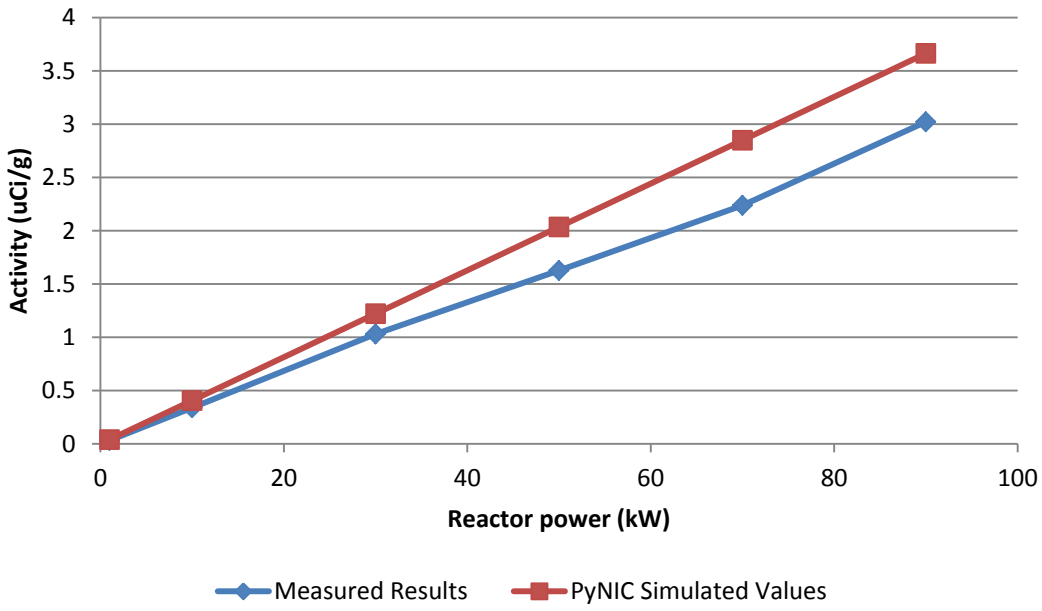

Figure 4.3. Measured NIST coal fly ash ^{56}Mn irradiation results and PyNIC simulated values vs. reactor power

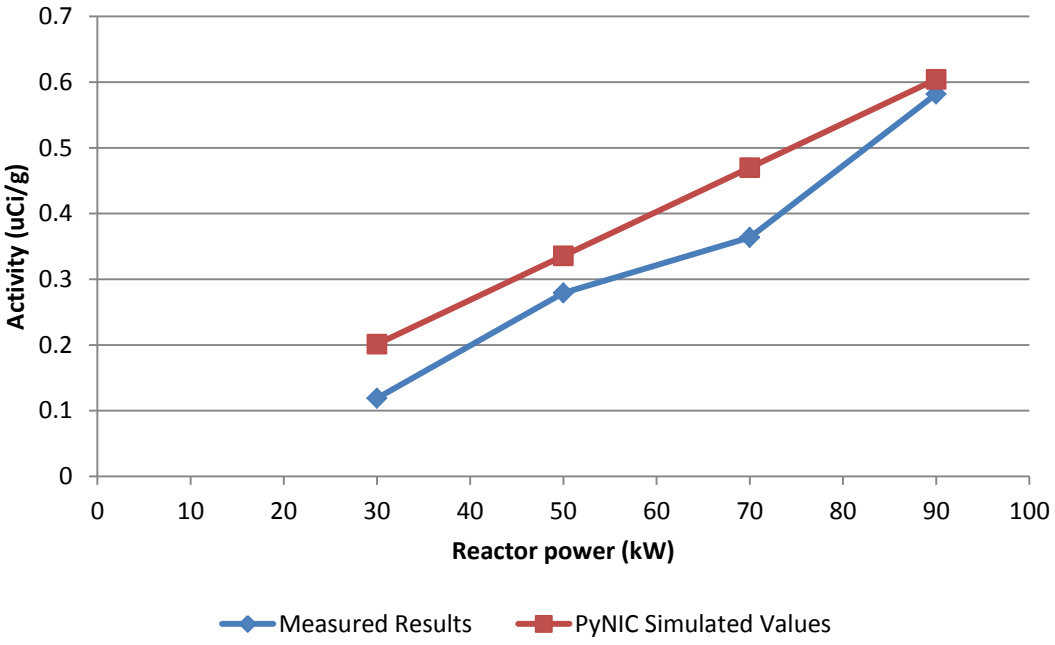

Figure 4.4. Measured NIST coal fly ash ^{40}K irradiation results and PyNIC simulated values vs. reactor power

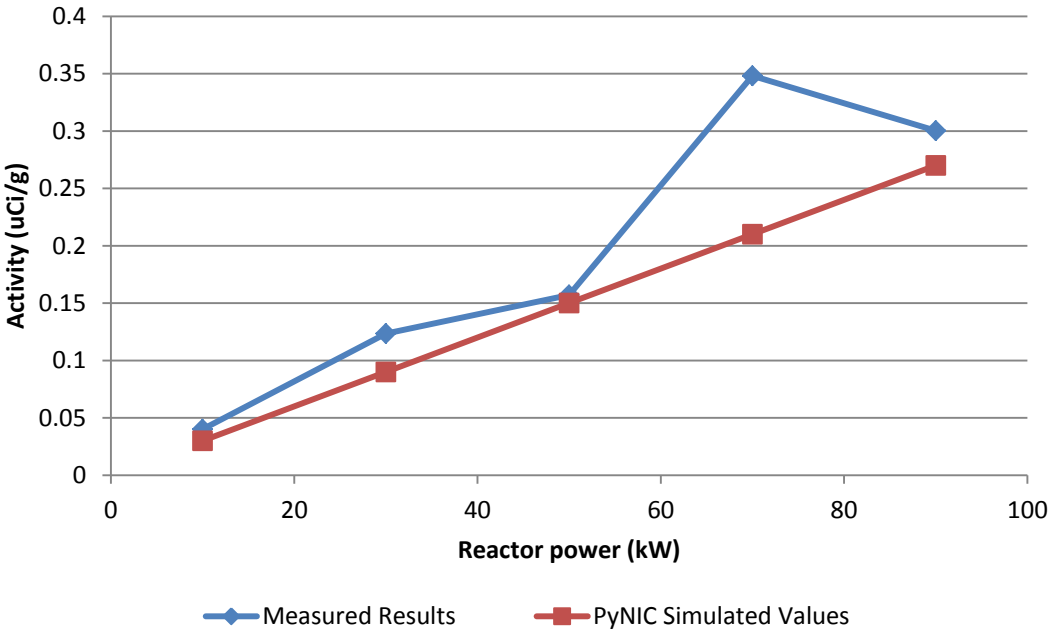

Figure 4.5. Measured NIST coal fly ash ^{139}Ba irradiation results and PyNIC simulated values vs. reactor power (explain why barium is bad)

Table 4.1 UUTR nickel sample irradiation parameters

Sample	Sample mass (g)	Power (kW)	Irradiation Time (min)	Decay Time (min)	Gamma Count Time (min)
1	0.1444	1	3	1.48	10
2	0.1046	1	3	17	10
3	0.0997	1	3	29	10
4	0.1021	10	3.57	53	10
5	0.1035	10	3.57	42	10
6	0.1101	10	3.57	65	10
7	0.1025	30	3	68	10
8	0.1023	30	3	79	10
9	0.1029	30	3	93	10
10	0.1041	50	3	96	10
11	0.1025	50	3	107	10
12	0.1024	50	3	120	10
13	0.1016	70	3	124	10
14	0.1017	70	3	136	10
15	0.1020	70	3	147	10
16	0.0954	90	3	139	10
17	0.1024	90	3	151	10
18	0.1021	90	3	162	10

Table 4.2 UUTR NIST coal fly ash standard irradiation parameters

Sample	Sample mass (g)	Power (kW)	Irradiation Time (min)	Decay Time (min)	Gamma Count Time (min)
1	0.1611	1	2	8.5	10
2	0.208	1	2	6	10
3	0.1886	1	2	11	10
4	0.1592	10	2	27	10
5	0.1312	10	2	33	10
6	0.1624	10	2	30	10
7	0.1648	30	2	44	10
8	0.1178	30	2	53	10
9	0.165	30	2	61	10
10	0.168	50	2	63	10
11	0.1325	50	2	68	10
12	0.1595	50	2.75	70	10
13	0.1249	70	2	73	10
14	0.0992	70	2	79	10
15	0.1087	70	2	80	10
16	0.0663	90	2	83	10
17	0.0447	90	2	87	10
18	0.0614	90	2	91	10

Table 4.3 UUTR nickel sample irradiation activity

Sample	^{65}Ni estimated activity (µCi/g)	^{65}Ni measured activity (µCi/g)	^{65}Ni measured activity +/- estimated by GENIE software (µCi)	Difference estimate from measured (µCi)	% difference of estimate from measured
1	0.25	0.24	0.04	0.02	6.85%
2	0.25	0.23	0.04	0.02	10.86%
3	0.25	0.24	0.04	0.01	4.52%
4	3.00	2.85	0.19	0.12	5.46%
5	3.00	2.92	0.20	0.07	2.88%
6	3.00	2.54	0.16	0.35	18.43%
7	7.59	7.38	0.41	0.15	2.77%
8	7.59	7.45	0.39	0.10	1.93%
9	7.59	7.59	0.37	0.00	-0.01%
10	12.65	12.72	0.60	-0.05	-0.58%
11	12.65	12.94	0.58	-0.18	-2.23%
12	12.65	12.63	0.54	0.01	0.14%
13	17.71	17.47	0.71	0.14	1.37%
14	17.71	17.51	0.68	0.11	1.15%
15	17.71	17.55	0.65	0.08	0.88%
16	22.77	22.36	0.85	0.22	1.82%
17	22.77	21.28	0.77	0.76	6.99%
18	22.77	22.04	0.75	0.35	3.31%

Table 4.4 UUTR NIST standard irradiation activity for ^{56}Mn

Sample	^{56}Mn estimated activity (µCi/g)	^{56}Mn measured activity (µCi/g)	^{56}Mn measured activity +/- estimated by GENIE software (µCi)	Difference estimate from measured (µCi)	% difference of estimate from measured
1	0.041	0.042	1.08E-02	-1.10E-03	-2.63%
2	0.041	0.036	8.58E-03	5.14E-03	14.46%
3	0.041	0.023	7.28E-03	1.79E-02	78.52%
4	0.41	0.35	2.91E-02	5.25E-02	14.81%
5	0.41	0.35	3.29E-02	6.06E-02	17.48%
6	0.41	0.32	2.62E-02	9.17E-02	29.08%
7	1.22	1.05	6.31E-02	1.71E-01	16.30%
8	1.22	1.03	6.20E-02	1.95E-01	18.98%
9	1.22	1.02	5.73E-02	2.06E-01	20.31%
10	2.04	1.61	8.58E-02	4.26E-01	26.43%
11	2.04	1.65	8.79E-02	3.90E-01	23.66%
12	2.79	2.35	1.18E-01	4.39E-01	18.66%
13	2.85	2.23	1.14E-01	6.19E-01	27.77%
14	2.85	2.18	1.11E-01	6.68E-01	30.60%
15	2.85	2.30	1.16E-01	5.49E-01	23.84%
16	3.66	2.99	1.52E-01	6.73E-01	22.52%
17	3.66	3.07	1.63E-01	5.96E-01	19.41%
18	3.66	3.01	1.52E-01	6.56E-01	21.81%

Table 4.5 UUTR NIST standard irradiation activity for ^{40}K (ND placed in Table when nuclide was not detected in sample)

Sample	^{40}K estimated activity (µCi/g)	^{40}K measured activity (µCi/g)	^{40}K measured activity +/- estimated by GENIE software (µCi)	Difference estimate from measured (µCi)	% difference of estimate from measured
1	ND	ND	ND	ND	ND
2	ND	ND	ND	ND	ND
3	ND	ND	ND	ND	ND
4	ND	ND	ND	ND	ND
5	ND	ND	ND	ND	ND
6	ND	ND	ND	ND	ND
7	0.20	0.083	5.38E-02	1.18E-01	141.44%
8	0.20	0.12	6.27E-02	7.80E-02	63.22%
9	0.20	0.15	5.82E-02	5.14E-02	34.30%
10	0.34	0.30	9.35E-02	3.06E-02	10.05%
11	0.34	0.25	8.56E-02	8.24E-02	32.55%
12	0.46	0.37	1.04E-01	9.07E-02	24.47%
13	0.47	0.27	1.05E-01	1.96E-01	71.40%
14	0.47	0.42	1.17E-01	4.80E-02	11.38%
15	0.47	0.40	1.24E-01	7.45E-02	18.85%
16	0.60	0.58	1.84E-01	2.45E-02	4.23%
17	ND	ND	ND	ND	ND
18	0.60	0.58	1.75E-01	1.98E-02	3.40%

Table 4.6 UUTR NIST standard irradiation activity for ^{139}Ba (ND placed in Table when nuclide was not detected in sample)

Sample	^{139}Ba estimated activity (µCi/g)	^{139}Ba measured activity (µCi/g)	^{139}Ba measured activity +/- estimated by GENIE software (µCi)	Difference estimate from measured (µCi)	% difference of estimate from measured
1	ND	ND	ND	ND	ND
2	ND	ND	ND	ND	ND
3	ND	ND	ND	ND	ND
4	0.030	0.037	2.75E-02	-7.32E-03	-19.61%
5	0.030	0.046	3.15E-02	-1.59E-02	-34.63%
6	0.030	0.037	2.82E-02	-6.88E-03	-18.66%
7	0.090	0.11	6.53E-02	-2.33E-02	-20.58%
8	0.090	0.14	7.39E-02	-4.89E-02	-35.20%
9	0.090	0.12	5.88E-02	-2.81E-02	-23.76%
10	0.15	0.16	7.70E-02	-1.24E-02	-7.61%
11	0.15	0.15	7.26E-02	-1.55E-03	-1.02%
12	0.21	0.24	1.06E-01	-3.14E-02	-13.23%
13	0.21	0.33	4.74E-02	-1.18E-01	-35.90%
14	0.21	0.36	1.46E-01	-1.46E-01	-40.97%
15	0.21	0.36	1.47E-01	-1.51E-01	-41.76%
16	0.27	0.26	1.18E-01	1.09E-02	4.21%
17	0.27	0.34	1.49E-01	-7.38E-02	-21.45%
18	0.27	0.30	1.28E-01	-2.77E-02	-9.31%

Table 4.7 UUTR nickel sample irradiation dose rate comparison

Irradiation	Total estimated dose rate after 1 minute (mrem/hr)	Measured dose rate after 1 minute (mrem/hr)	Difference estimate from measured (mrem/hr)
1	0.00052	0.01	0.0095
2	0.0055	0.01	0.0045
3	0.0136	0.12	0.11
4	0.023	0.11	0.087
5	0.032	0.20	0.017
6	0.040	0.19	0.15

Table 4.8 UUTR NIST sample irradiation dose rate comparison

Irradiation	Decay Time (min)	Total estimated dose rate (mrem/hr)	Measured dose rate (mrem/hr)	Difference estimate from measured (mrem/hr)
1	1	0.077	0.02	0.057
2	1	0.099	0.03	0.069
3	1	0.09	0.01	0.08
4	1	0.76	0.68	0.08
5	1	0.63	0.35	0.28
6	1	0.78	0.43	0.35
7	2	1.74	3.4	-1.66
8	1	1.69	2.04	-0.35
9	6	0.51	0.45	0.06
10	3	2.17	2.15	0.02
11	5	0.93	0.8	0.13
12	4	1.89	2.1	-0.21
13	3	2.26	1.35	0.91
14	6	0.72	0.9	-0.18
15	4	1.45	1.2	0.25
16	5	0.84	0.9	-0.06
17	4	0.77	1.1	-0.33
18	6	0.57	0.65	-0.08

CHAPTER 5

APPLICATIONS OF PyNIC

5.1 Nuclear Fuel Interrogation Simulated with MCNPX and PyNIC

This chapter is for explaining the different applications of PyNIC. Its purpose is for the user to draw inspiration on how it can be used in the fields of nuclear power, nuclear medicine, and nuclear security. The approach using PyNIC to active neutron interrogation of used nuclear fuel is to take real neutron energy spectrum measurements (or an MCNPX (Monte Carlo N-Particle, version X) (*32*) simulated neutron energy spectrum) and build it into the calculator. MCNPX is a radiation transport code based on Monte Carlo methods combined with neutron cross section data libraries to simulate the transport and secondary particles generated from neutrons. The Python tool, PyNIC, can be used to simulate the fuel interrogation of a wide range of fuel types and fuel content. This would be accomplished by entering the isotopic abundance of a fuel type into the GUI and then running the calculations to determine the gamma emissions from ^{235}U, ^{238}U, or ^{239}Pu fission or from the neutron absorption inn cladding material. These gamma emissions are then built into an MCNPX input file for modeling the gamma spectrum on a HPGe detector by the simulation tool. The same tool also plots the gamma spectrum after completion of the MCNPX simulation. The plots can then be generated for a wide

range of fuel content and used to compare to real measurements to ascertain the content of the fuel. One current shortcoming of the tool for fuel interrogation is the fission product gamma emissions are not accounted for currently. This could be part of the future work and added in the future.

5.2 Simulation Model of Neutron Capture Therapy with Compact Neutron Generators

The modeling of compact neutron sources for NCT is another potential use of the calculator. The initial modeling of the source and moderating material would be done using MCNPX (*32*). These sources can then be used with a model developed from real patient computerized tomography (CT) scan data to model dose distributions in the patient (*33*). The subsequent analysis of the dose distributions simulated in MCNPX can be performed using CERR: A Computational Environment for Radiotherapy Research (version beta 4) (*34*), an open source library implemented in Matlab®. CERR overlays the dose distributions on the patient CT data. The combination of these different tools leads to accurate representations of neutron scattering and dose deposited in a patient.

Two different compact neutron generator models were looked at for their potential in the BNCT simulations. Both models are based on a neutron multiplier model proposed by Rasouli and Masoudi (*35*). Their model uses a sphere of uranium metal to increase neutron flux generated by the D-T reaction through fission of the uranium. The models used in this work were recreated with slight modifications using MCNP5. The first model, shown in Fig. 5.1, has only slight modifications from their original work. The second model does not use the sphere of uranium to multiply the neutrons but does use

the same moderating materials with some modifications. Each of these sources is modeled to record neutrons exiting the aperture focused towards the patient to be used in the dose simulations with the patient CT data. The flux from the neutron multiplier model is shown in Fig. 5.2.

Once recorded, the neutrons from these two sources can be used to simulate the dose to a patient with HER2+ breast cancer. The patient model, constructed in MCNPX from real CT data of a female patient (*33*), allows for highly accurate predictions of neutron scattering and capture in the patient. It also allows for highly accurate estimates of dose distributions in the tumor and surrounding healthy tissue, which are crucial in determining the effectiveness of the neutron beam and the treatment. The Massachusetts Institute of Technology Fission Converter Beam (MITII-FCB), which is an epithermal neutron beam (*36*), is another potential source that could be used to simulate the dose distributions to compare compact neutron source to a beam from a research reactor. The reported in-air epithermal neutron flux for the MITII-FCB beam is between $3.2x10^9$–$4.6x10^9$ n/(cm^2s) (*37*), while the flux for the neutron multiplier at the aperture is in the range of 10^8 or 10^9 n/(cm^2s) depending on the neutron generation rate in the target. Maximizing the neutron flux from the neutron generator is a key component to effective neutron capture therapy.

Fig. 5.3 shows the simulated dose distribution across the patient from the neutron multiplier beam. The dose is tallied across many small voxels to generate Fig. 5.3. The neutron energy spectrum and flux can also be tallied across each of those voxels during the simulation. Then, once the simulation, which can be very computationally expensive, has been performed once, the measured neutron energy spectrum and flux can be used in

the PyNIC to model the interactions that occur and more specifically the number of neutron captures that occur in ^{10}B for a given concentration of ^{10}B. The calculated number of neutron captures in ^{10}B determines the Li ion and alpha particle flux and energy in the tumor, which can then be used to perform calculations on the RBE of the beam using a separate program called MCDS. This calculation can be repeated rapidly for a number of different ^{10}B concentrations without having to repeatedly rerun MCNPX simulations.

5.3 Modeling of Compact Neutron Generators in Homeland Security – Explosives Detection

The proposed concept for simulating explosives detection using active neutron interrogation uses a combination of MCNPX and the Python scripts to simulate the gamma signatures observed in a sample of explosive material. The first step would be the simulation of the neutron fluence and energy spectrum inside the sample using MCNPX. The second step involves using the simulated neutron fluence and energy spectrum in the Python-based neutron interaction simulator to calculate the gamma signatures that would be created through neutron capture and select inelastic scattering events. These calculated values are then used in a simplified MCNPX input file to simulate the gamma signature on a germanium crystal. This method significantly reduces the computational time needed to run a real case scenario MCNPX input file. These simulations could be performed for a wide range of explosive materials to provide data for comparison to real measurements.

5.4 Modeling of Compact Neutron Generators in Homeland Security – Special Nuclear Material Detection

The proposed concept for simulating the detection of highly enriched uranium is similar to that for explosive material except that the gamma signature contribution from fission has to be considered. This is built into the Python simulation tool so additions to the gamma signature from fission can be correctly calculated. A range of special nuclear materials could be tested including a range of uranium enrichments, plutonium enrichments, and a combination of both uranium and plutonium. In addition, different thicknesses of shielding could also be tested to simulate the effects shielding would have on detection of each material.

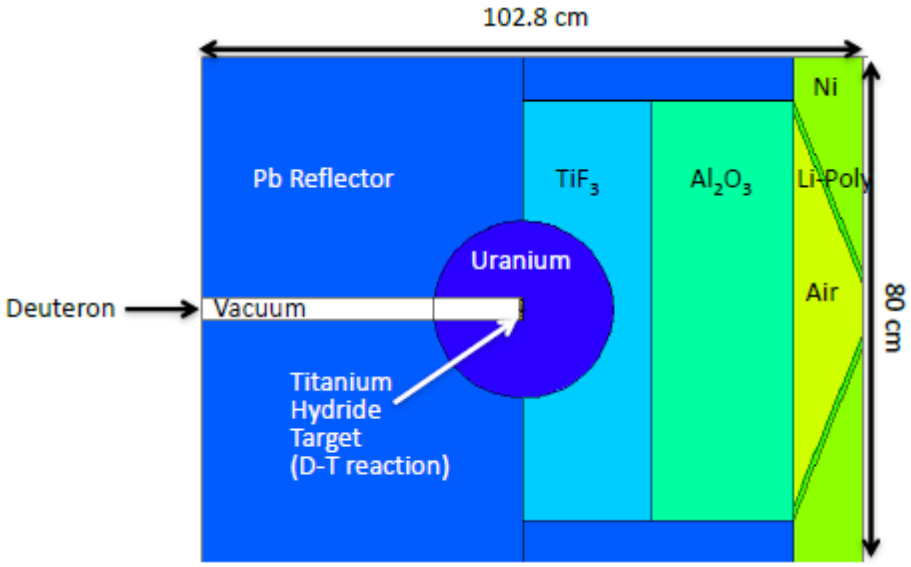

Figure 5.1. Neutron multiplier model

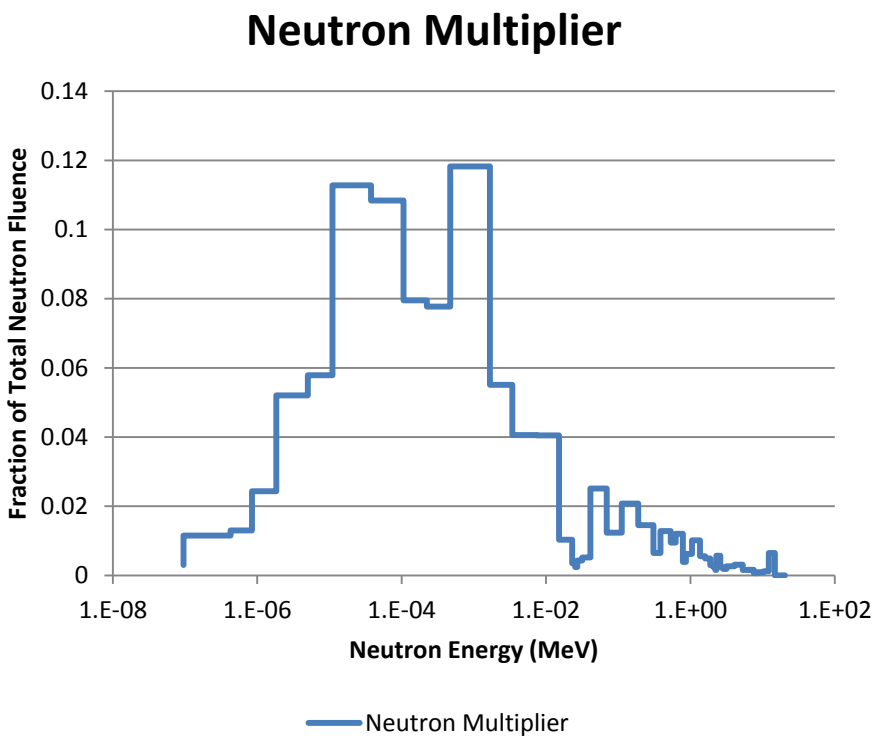

Figure 5.2. Neutron energy spectrum of neutron multiplier model

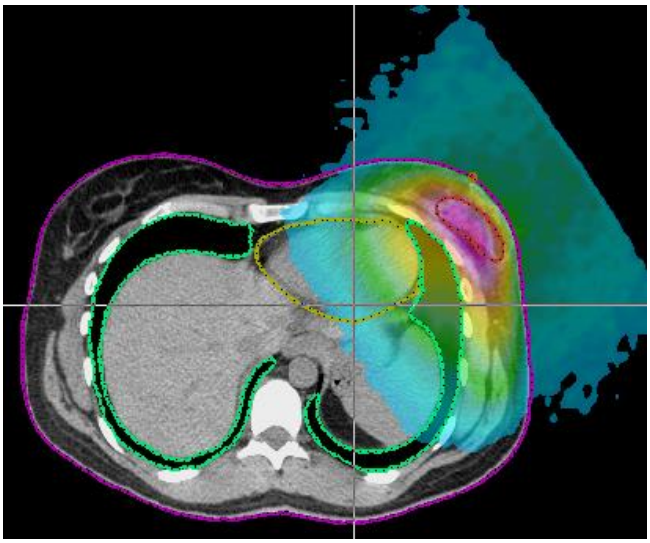

Figure 5.3. Dose distribution from neutron multiplier beam

CHAPTER 6

CONCLUSIONS AND FUTURE WORK

The PyNIC tool has great potential for modeling the neutron interactions relevant to nuclear power, nuclear medicine, and homeland security applications, not to mention applications in neutron activation analysis practiced at labs across the world. The tool offers the advantage of using the entire neutron cross section library for its neutron capture, neutron inelastic scattering, and fission events compared to just using the cross section at a thermal energy of 0.025 eV to calculate the rate of neutron capture in the defined media. This allows for a more accurate calculation of the interactions occurring because all neutron energies are considered. The tool allows for the testing of different neutron spectrums with computation times on the order of seconds instead of having to run long simulations to test those same spectrums for the given application. Also, after the calculations are made for neutron capture, an MCNPX simulation can then be performed of the HPGe detector response from the gamma emissions (either the instantaneous gamma emissions or the delayed emissions from the radioactive daughter products). This allows the user to have easy access to what gamma spectrum they would expect from a sample for their given neutron energy spectrum. It also allows for design of a neutron beam that will help maximize the desired gamma emissions they want when looking for given atomic constituents in a sample.

Future work includes the continued benchmarking of PyNIC through additional NAA experiments. These include irradiations of gold, silver, titanium, tungsten, molybdenum, aluminum, iron, copper and many other metal wire samples. The evaluation of the gamma emission rates for prompt neutron analysis would also be a valuable future project to ensure that the code is benchmarked for immediate gamma emissions after the exposure of a sample to a neutron beam. Also, to help improve the activity predictions, improvements to the cross section library processing algorithm need to be made. The first improvement needed is to use the average neutron energy across the bin instead of the top energy limit of the bin. Also, how the cross section is calculated for a given energy bin needs improvement for better accuracy.

The PyNIC has the potential for many great additions to increase its applications in nuclear engineering. One such addition would be to increase the number of nuclides the user can select from five to as many as they need, thereby allowing the user to perform all the calculations at once for samples with many constituents. Another addition that would be valuable would be to add inelastic scattering cross sections (and the instantaneous gamma emissions) for more nuclides so that the interactions can be factored into the gamma spectrum a user could expect.

An addition that would be valuable when modeling the gamma emissions that would occur during active fuel interrogation would be to have the option to add the fission product gamma emissions for the fuel instead of just getting the gamma rays emitted from immediate neutron interactions. This would help simulate a much more accurate gamma spectrum from used fuel. The combination of these new additions would be

highly valuable in extending the applicability of the Python based neutron interaction simulator tool to more fields in nuclear engineering.

APPENDIX A

PYTHON SCRIPTS

GUI_NAA.py

- Builds user interface
- Sends user input to NAA_Report_generator.py through *reports* function
- Sends user input to HPGe_Input_write.py through *HPGe_write* function

NAA_Report_generator.py

- Generates report of neutron interactions
- Contains the neutron energy spectrum and flux of any neutron beams built into the PyNIC
- Sends user selected nuclides to Nuclide_Data.py to select appropriate cross sections, half-lives, and activation products based on user selected nuclides
- Sends entire cross section data to XS_Function.py to process the cross section data according to the energy spectrum of the neutron beam
- Sends neutron flux, neutron energy, processed cross section data, irradiation time, decay time, nuclide half-lives, and number of parent nuclides to Activity_Function.py to calculate activity for each user selected nuclide
- Sends user selected nuclides to Dose_Data.py to select appropriate gamma emission rates for the user selected nuclides
- Sends gamma decay data for each activation product to Mass_atten_calculator.py to calculate the appropriate attenuation factors based on the gamma emissions from the sample
- Sends nuclide activity, gamma emission data, and mass attenuation factors to Dose_Function.py to calculate dose rates based on gamma emissions from the activation products

- Returns the results of calculations back to GUI_NAA.py

Activity_Function.py

- Calculates the activity for each user selected nuclide and neutron beam
- Calculates the instantaneous gamma ray emission rates from neutron capture, fission, and neutron inelastic scattering
- Returns the results of these calculations to NAA_Report_generator.py

Dose_Data.py

- Contains gamma emission data for neutron capture, inelastic scattering, and fission
- Returns this data to NAA_Report_generator.py

Dose_Function.py

- Calculates the dose the user would expect at 1 foot from the gamma emissions of the activation products
- Returns the results of these calculations to NAA_Report_generator.py

HPGe_Input_write.py

- Uses gamma emission rates calculated and returned to GUI_NAA.py to build an MCNPX input file for the simulation of the gamma spectrum one would expect from a given sample on a HPGe detector
- Writes a text file named Isotope.txt

HPGe_Report_generator.py

- After a MCNPX run of the HPGe input file has been completed and the "Generate HPGe Report" button has been pressed, the HPGe_Report_generator.py script extracts the results from the MCNPX output file and generates a plot and a report

with those results

Mass_atten_calculator.py

- Calculates the attenuation factors for the gamma rays emitted from a sample
- Returns these values to NAA_Report_generator.py

Nuclide_Data.py

- Contains the activation products, the half-lives, and masses for the nuclides contained in PyNIC
- Imports cross section data for user selected nuclides from the nuclide's individual file (i.e. for ^{1}H the file is H1.py)
- Returns nuclide data back to NAA_Report_generator.py

XS_Function.py

- Processes nuclide cross section to set up an energy spectrum that is the same as the neutron beam energy spectrum
- Returns to NAA_Report_generator.py

APPENDIX B

HPGE MCNPX INPUT FILE

```
Isotope Input File
C ***********************************************************************
C ******************************Section 1, Cell
Cards*********************
C ***********************************************************************
1    2 -5.35 1 -2 -3       $germanium crystal
2    0 -99   (-1:2:3)      $universe boundary
99   0          99         $outside universe boundary

C ***********************************************************************
C ******************************Section 2, Surface
Cards*******************
C ***********************************************************************
1    PZ 0                   $crystal Front
2    PZ 3.68                $back of crystal
3    CZ 3.355               $crystal radius
99   SO 600                 $SPHERE DEFINING THE BOUNDARY OF THE UNIVERSE

C ***********************************************************************
C ***Section 3, Particle Physics, Importances, Mode, Energy Cutoffs,
Var. Red., etc.)**
C ***********************************************************************
MODE P
imp:p 1 1 0
C ***********************************************************************
C ********************************Section 4, Material
Cards***************
C ***********************************************************************
M2   32000 1.0      $ Ge (5.35 g/cc)
C ***********************************************************************
C ******************************Section 5, Source
Definition*****************
```

```
C ********************************************************************
SDEF   ERG=D3
       POS= 0 0.0 -10
       VEC= 0 0.0 1
       DIR=D1
       RAD=D2
       WGT=0.01
SI1    0.98 1
SP1    0 1
SI2    0 0.05
SI3 L 1.77885
SP3   1.0
C ********************************************************************
C ******************************Section 6, Tally
Definition******************
C ********************************************************************
F8:P 1
E8   0 1.E-6 1.E-3 8196I 3.0
FT8 GEB 0 0.0017 0
C ********************************************************************
C ******************Section 7, Simulation Control and Debug
Parameters*********
C ********************************************************************
nps  1e8
```

APPENDIX C

NEUTRON INTERACTION REPORT

==========

UNEP NAA Calculator Version 1.00B 9-October-2013

==========

Table 1. Activation Products

==========

Nuclide	Activity (mCi)	Half-life (minutes)
Ni-65	0.307906553906	151.032
Na-24	0.0510247278134	897.54
Mg-27	0.243292748802	9.458
Al-28	2.90446595108	2.2414
K-42	0.0	741.6
Total	3.5066899816	

Table 2. Calculated Dose

==========

Nuclide	Dose Rate (mrem/hr)
Ni-65	1.76683768768
Na-24	1.66735797539
Mg-27	2.66631997887
Al-28	44.9797304325
K-42	0.0

Total 51.0802460744

Table 3. Gamma Emissions from Ni-65

Gamma Energy (MeV)	Decay Ratio (per radioactive decay of Ni-65)
1.48184	0.2359
1.11553	0.1542786
0.36627	0.04805283
1.62342	0.00497749
1.72492	0.00398671

Table 4. Gamma Emissions from Na-24

Gamma Energy (MeV)	Decay Ratio (per radioactive decay of Na-24)
1.368633	1
2.754028	0.99944
3.86619	0.00052
0.99682	1.4e-05
4.23796	1.1e-05

Table 5. Gamma Emissions from Mg-27

Gamma Energy (MeV)	Decay Ratio (per radioactive decay of Mg-27)
0.84376	0.718
1.01444	0.28
0.170686	0.008

Table 6. Gamma Emissions from Al-28

Gamma Energy (MeV)	Decay Ratio (per radioactive decay of Al-28)
1.77885	1

Table 7. Gamma Emissions from K-42

Gamma Energy (MeV)	Decay Ratio (per radioactive decay of K-42)
1.5247	0.1808
0.3126	0.00336288
0.89943	0.00051528
1.92218	0.000412224
1.02278	0.000200688

Table 8. Instantaneous Gamma Emission rate

Nuclide	Gamma emission per second
Ni-65	504499424.159
Na-24	490246361.307
Mg-27	31572281.1092
Al-28	186047696.846
K-42	4187101465.06
Total	5399467228.49

Table 8. Instantaneous Gamma Emissions from Ni-64

Gamma Energy (MeV)	Decay Ratio (per gamma caputre in Ni-64)
6.0348	0.67
0.3102	0.220028
5.7878	0.177014
0.0636	0.119997
5.4058	0.088976

Table 9. Instantaneous Gamma Emissions from Na-23

Gamma Energy (MeV)	Decay Ratio (per gamma capture in Na-23)
0.4722	0.9039
0.09099	0.44526114
0.86923	0.20419101
6.39538	0.18376287
0.8744	0.14362971

Table 10. Instantaneous Gamma Emissions from Mg-26

Gamma Energy (MeV)	Decay Ratio (per gamma capture in Mg-26)
2.88167	0.6554
3.56131	0.60159166
1.61528	0.16902766
0.98491	0.15618182
6.4425	0.09188708

Table 11. Instantaneous Gamma Emissions from Al-27

Gamma Energy (MeV)	Decay Ratio (per gamma capture in Al-27)
0.03064	0.279

7.72403	0.2680074
3.03389	0.0879966
3.46507	0.0700011
4.13341	0.0689967

Table 12. Instantaneous Gamma Emissions from K-41

Gamma Energy (MeV)	Decay Ratio (per gamma capture in K-41)
0.10682	0.33
0.68193	0.155001
0.8419	0.132
0.15143	0.106986
5.16728	0.066

REFERENCES

1. International Atomic Energy Agency. *Neutron generators for analytical purposes;* International Atomic Energy Agency: Vienna, 2012.

2. Csikai, J. *Handbook of Fast Neutron Generators;* CRC Press: Boca Raton, 1987; Vol. I.

3. Chichester, D. L.; Simpson, J. D. *Compact accelerator neutron generators;* Thermo Electron Corp.: Colorado Springs, 2003.

4. Berkeley Lab. Berkeley Lab, Lawrence Berkeley National Lab. http://www.lbl.gov/Tech-Transfer/techs/lbnl1764.html#Cylindrical (accessed October 26, 2013).

5. Williams, D. L.; Vainionpaa, J. H.; Jones, G.; Piestrup, M. A.; Gary, C. K.; Harris, J. L.; Fuller, M. J.; Cremer, J. T.; Ludewigt, B. A.; Kwan, J. W.; Reijonen, J.; Leung, K.-N.; Gough, R. A. High intensity, pulsed, D-D neutron generator. *Application of Accelerators in Research and Industry: 20th International Conference*, Fort Worth, 2009; pp 936–939.

6. B. H. Armitage, K. P. Lambert, M. T. Swinhoe. *Development of non-destructive actinide assay methods for radioactive waste;* AEA Technology: Harwell, United Kingdom,1990.

7. S.J. Tobin, et al. *Determining plutonium mass in spent fuel with non-destrucive assay techniques - NGSI research overview and update on NDA techniques, part I;* Los Alamos National Lab: Los Alamos, 2010.

8. Campbell, L. W.; Smith, L. E.; Misner, A. C. High-energy delayed gamma spectroscopy for spent nuclear fuel assay. *IEEE Trans. Nucl. Sci.* **2011,** *58* (1), 231–240.

9. Korea Atomic Energy Research Institute. Table of nuclides. http://atom.kaeri.re.kr/ (accessed October 26, 2013).

10. Harling, O. K. Fission reactor based epithermal neutron irradiation facilities for

routine clinical application in BNCT-Hatanaka memorial lecture. *Appl. Rad. Iso.* **2009,** *67,* S7–S11.

11. Mundy, D.; Harb, W.; Jevremovic, T. Radiation binary targeted therapy for Her-2+ positive breast cancers: assumptions, theoretical assesment and future directions. *Phys. Med. Bio.* **2006,** *51,* 1377–1391.

12. Chen, Y.-B. Breast cancer. http://www.nlm.nih.gov/medlineplus/ency/article/000913.htm (accessed October 26, 2013).

13. Pruthi, S. HER2-positive breast cancer: What is it? http://www.mayoclinic.com/health/breast-cancer/AN00495 (accessed October 26, 2013).

14. Lanza, R. C. *Counterterrorist Detection Techniques of Explosives*, 1st ed.; Elsevier B. V.: Oxford, 2007.

15. Jevremovic, T. *Nuclear Principles in Engineering*, 2nd ed.; Springer: West Lafayette, 2009; Vol. 1.

16. David Koltick, S. M. A neutron based vehicle borne improvised explosive device detection system. *Security Technology, 2007 41st Annual IEEE International Carnahan Conference on*, Ottawa, 2007; pp 292–300.

17. Chichester, D. L.; Thompson, S. J.; Seabury, E. H.; Clement, R. R. C. Parametric evaluation of active neutron interrogation for the detection of shielded highly-enriched uranium in the field. *2011 IEEE Nuclear Science Symposium Conference Record*, Valencia, 2011; pp 964–971.

18. England, T. R.; Rider, B. F. *Evaluation and compilation of fission product yields*; Los Alamos National Lab: Los Alamos, 1993.

19. Weinstein, S. T. *NAC: neutron activation code*; NASA Technical Memorandum; National Aeronautics and Space Administration: Washington DC, 1968.

20. Forschungs-Neutronenquelle Heinz Maier-Leibnitz (FRM II). FRM II neutron activation calculator. http://www.frm2.tum.de/intranet/activation/ (accessed May 7, 2014).

21. National Institute of Standards and Technology (NIST). Neutron activation and scattering calculator. http://www.ncnr.nist.gov/resources/activation/ (accessed May 7, 2014).

22. WISE Uranium Project. Neutron activation calculator. http://www.wise-uranium.org/rnac.html (accessed May 7, 2014).

23. Agency, I. A. E. Thermal neutron capture gamma-rays. http://nucleus.iaea.org/CIR/CIR/ThermalNeutronCaptureGammarays.html (accessed January 28, 2014).

24. Hall Jr., H. E. Neutron inelastic scattering in C-12, N-14, and O-16; Ph.D. Thesis, The Rice Institute, Houston, April, 1959.

25. Agency, I. A. E. Average number of neutrons emitted per fission. https://www-nds.iaea.org/sgnucdat/a6.htm (accessed April 2, 2014).

26. Cember, H.; Johnson, T. E. *Introduction to Health Physics*, 4th ed.; McGraw-Hill: New Baskerville, 2009; Vol. 1.

27. Technology, N. I. o. S. a. X-ray mass attentuation c oefficients. http://physics.nist.gov/PhysRefData/XrayMassCoef/ComTab/air.html (accessed January 28, 2014).

28. Hunter, J. D. Matplotlib: A 2D graphics environment. *Comp. Sci. Eng.* 2007, 9 (3), 90–95.

29. National Institute of Standards and Technology. *Standard reference material 1633c*; Certificate of analysis; National Institute of Standards and Technology, Gaitherburg, MD, 2011.

30. National Institute of Standards and Technology. *Standard reference material 2710a*; Certificate of analysis; National Institute of Standards and Technology, Gaithersburg, MD, 2009.

31. National Institute of Standards and Technology. *Standard reference material 1573a*; Certificate of analysis; National Institute of Standards and Technology, Gaithersburg, MD, 1995.

32. Team, X.-5. M. C. MCNP – A general Monte Carlo n-paricttle transport code, version 5; Los Alamos National Laboratory, Los Alamos, 2005.

33. Jenkins, P. BNCT for HER2+ Breast Cancers, A Feasibility Study Evaluating BNCT for Potential Role in Breast Conservation Therapies; Ph.D. Thesis, University of Utah, Salt Lake City, 2012.

34. Deasy, J. O.; Blanco, A.; Clark, V. H. CERR (A computational environment for radiotherapy research). *Med. Phys.* 2003, 30, 979–985.

35. Rasouli, F. S.; Masoudi, S. F. Design and optimization of a beam shaping assembly for BNCT based on D-T neutron generator and dose evaluation using a simulated head phantom. *Appl. Rad. Iso.* 2012, 70, 2755–2762.

36. Riley, K. J.; Binns, P. J.; Harling, O. K. A state-of-the-art epithermal neutron irradiation facility for neutron capture therapy. *Phys. in Med. and Bio.* 2004, 49, 3725–3735.

37. MIT. MIT BNCT. http://web.mit.edu/nrl/www/bnct/facilities/FCB/fcb.html (accessed October 17, 2013).

38. Verbeke, J. M.; Vujic, J. L.; Leung, K. Neutron beam optimization for boron neutron capture therapy using the D-D and D-T high-energy neutron sources. *Rad. Bio. Med.* 2000, 129, 257–278.

39. Hall, E. J.; Giaccia, A. J. *Radiobiology for the Radiologist*, 6th ed.; Lippincott Williams and Wilkins: Philadelphia, 2006.

40. Nuclear chain reaction. http://chemistry.tutorvista.com/nuclear-chemistry/nuclear-chain-reaction.html (accessed December 9, 2013).